# THE IMPORTANCE OF MUSCLE MECHANICS DURING MOVEMENT: INVESTIGATING POWER PRODUCTION AND DYNAMIC STABILITY USING A CLOSED-LOOP SYSTEM

A Dissertation
Presented to
The Academic Faculty

By

Kartik Sundar

In Partial Fulfillment
of the Requirements for the Degree
Doctor of Philosophy in the
School of Biomedical Engineering

Georgia Institute of Technology
May 2009

**THE IMPORTANCE OF MUSCLE MECHANICS DURING MOVEMENT: INVESTIGATING POWER PRODUCTION AND DYNAMIC STABILITY USING A CLOSED-LOOP SYSTEM**

Approved By:

Dr. Stephen P. DeWeerth, Advisor
School of Biomedical Engineering
*Georgia Institute of Technology*

Dr. Lena H. Ting, Advisor
School of Biomedical Engineering
*Georgia Institute of Technology*
*Emory University*

Dr. Thomas J. Burkholder
School of Applied Physiology
*Georgia Institute of Technology*

Dr. T. Richard Nichols
School of Applied Physiology
*Georgia Institute of Technology*

Dr. Matthew C. Tresch
Department of Physical Medicine and Rehabilitation
*Northwestern University*

Date Approved: 01/20/2009

To my family

# ACKNOWLEDGEMENTS

I could not have completed this work without an enormous amount of support from a variety of people. I would like to thank the DeWeerth and Ting groups for their insights, creativity, and most importantly, friendships – I enjoyed all our interactions. I want to especially thank those who have had a large impact on my professional growth: Edgar Brown, Shane Migliore, Jim Ross, and Jevin Scrivens took the time to help me develop my practical engineering skills; Nate Bunderson, Lucas McKay, and Gelsy Torres-Oviedo always made themselves available to discuss the scientific content of this work. I would like to thank my advisors, Steve DeWeerth and Lena Ting, who taught me a wealth of knowledge that will aid me throughout my career. They consistently worked to ensure my rapid professional development. I would also like to thank Tom Burkholder, a member of my thesis committee, for his generous commitment towards my progress. My other thesis committee members, Richard Nichols and Matt Tresch, thank you for your valuable insights and direction. I would like to thank my family, who has been a source of continual support throughout my career. Finally, I would like to thank my fiancée, Rekha Nair, for her unwavering love and dedication. Thank you for reminding me of my accomplishments during the worst of times and pushing me to improve myself during the best of times.

# TABLE OF CONTENTS

# LIST OF TABLES

# LIST OF FIGURES

# SUMMARY

Animals effectively move and negotiate a variety of environments exemplifying the neuromuscular system's ability to produce complex coordinated movements. Our central thesis is that the nonlinear dynamical properties of muscle play a critical role in power production and stability during such movements. We have developed a closed-loop system that couples an isolated muscle to a physical or computational load, facilitating the study of the interactions between intrinsic muscle properties and external forces. We used this system to determine how elastic elements in the frog semimembranosus can improve power production during a jumping task and how the contractile element automatically manages energy to maintain a stable bouncing gait. Our results reveal that, during ballistic movements (e.g. jumping), series elastic elements stretch and shorten to temporally concentrate energy transfer from the contractile element to the body, amplifying power production. We measured peak instantaneous power greater than twice the maximum power the contractile element could produce alone. Our results show how, during a bouncing gait, the contractile and elastic elements autonomously interact to produce, dissipate, and recycle energy and to maintain dynamic stability without sensory feedback. Our data suggest that muscles can recover over 75% of the kinematic energy from one step and apply it to the next. These results demonstrate the effects and importance of intrinsic muscle properties during movements. Ultimately, this research can guide the development of biomimetic robotic and prosthetic technologies capable of life-like mobility.

# CHAPTER 1

# INTRODUCTION

## Overview

The ability of animals to effectively move and negotiate different environments is typical of the facilities of neuromuscular systems to solve complex problems beyond the capabilities of any engineered system. The inability of robotic systems to efficiently and autonomously move limits their contribution in medical and consumer applications. Investigating the emergent properties of the animal neuromuscular system can further our understanding of the function and architecture of the nervous system, and in addition, may allow us to design and construct improved robotic systems (Caldwell and Tsagarakis, 2002; Herr et al., 2001; Loeb, 2001). The neuromuscular system executes movements and interacts with the environment with muscles. The mechanical properties of muscle may provide a capable foundation for robust animal movement that simplifies the control requirements of the nervous system. However, the particular muscular strategies used during movement are not fully understood. In this dissertation, we examine how the mechanical properties of muscle effectively produce energy and stabilize locomotion using a closed-loop system.

In our first scientific study, we investigate the role of elastic elements in muscle within the context of frog jumping, using as an exemplar muscle the frog semimembranosus (SM). Animals have evolved neuromuscular strategies that take advantage of the mechanical properties of muscle during movement. The physics associated with an

effective isolated jump require maximizing power production making jumping a good system in which to examine an optimal neuromuscular strategy. We hypothesize that series elastic elements (SEEs) can function to temporally concentrate energy transfer from the contractile element (CE) to the body and enhance power production during a jump. Further, we examine the effect of different jump strategies on muscular power production. Our results demonstrate that the different mechanical elements in muscle function together in a specific temporal pattern to produce, store, and release energy enhancing power production during a jump. In addition, our results highlight the effect that even simple neuromuscular strategies can have on movement performance.

In our second scientific study, we hypothesize that the intrinsic properties of muscles, without the aid of the nervous system, can stabilize a bouncing gait. In natural environments, animals continuously withstand unexpected mechanical perturbations with unparalleled agility during locomotion. We test whether the intrinsic properties of muscle, without sensory feedback, were sufficient to form a stable limit cycle during a bouncing gait. Our results reveal how the different mechanical elements of muscle function to generate, dissipate, store, and release energy to maintain dynamic stability.

We use a combination of experimental and computational techniques to exhaustively test our hypotheses. We designed and employed a novel experimental apparatus that dynamically couples an isolated muscle to an arbitrary mechanical environment – a physical mechanical system, a simulated system, or a convenient combination of the two. This apparatus improves upon traditional methods and facilitates the study of a living muscle during dynamic movements. In addition, a computational muscle model was

developed to allow us to extrapolate how different muscular properties, that are unattainable through experimental methods, may affect performance.

We demonstrate that the mechanical properties of muscle facilitate the robust capabilities of animal movement and suggest that duplicating these properties in engineered systems will improve their performance. In this chapter, we give a brief introduction to muscle physiology, energetics, stability, and potential applications.

## Mechanical Feedback Can Define Muscle Function During Movements

Movement is the result of the coordinated interactions between the central nervous system, the musculoskeletal system, and the physical environment (Figure 1.1) (Dickinson et al., 2000). The central nervous system, subject to time delays, uses sensory information about the body and environment to plan and execute movements. Muscles, a primary component of the musculoskeletal system, are controlled by the central nervous system to apply forces to the body during movement. In addition to activation, the forces produced by muscles are also subject to the mechanical feedback, the instantaneous interactions between musculoskeletal system and the physical environment. In this dissertation, we focus our study on the interactions between the mechanical properties of muscle and the physical environment.

During locomotion the neuromuscular system employs global strategies to minimize energetic expenditure. For example, in walking gaits, the body acts like a pendulum, exchanging kinetic and gravitational energy during every step which reduces the energetic cost (Cavagna et al., 1977). During rapid forms of locomotion, such as

running, the limbs act like springs, exchanging kinetic and gravitational energy with elastic energy (Alexander and Bennet-Clark, 1977; McMahon and Cheng, 1990). Although the overall strategies are simple, the functions of individual skeletal muscles, which produce the movements, are more complex.

During movements, muscles operate in three primary modes: (1) as motors, (2) as brakes, or (3) as struts (Dickinson et al., 2000). Traditionally, muscles were thought of as motors that produce energy and accelerate the body during locomotion. For example, during a jump, the hindlimb muscles in a frog produce force and shorten to generate energy (Lutz

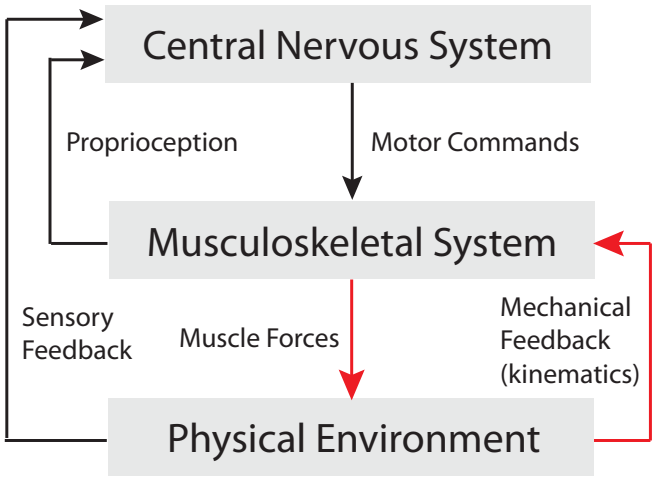


**Figure 1.1: Movement is the result of a coordinated effort by the neuromuscular system.** The central nervous system generates motor commands to activate the muscles, which belong to the musculoskeletal system. In turn, the activated muscles generate forces and act on the physical environment, producing movement. The force produced by muscles can be modified by both sensory and mechanical feedback to control movement. In this dissertation, we demonstrate the importance and effects of mechanical feedback (red lines) on muscular function and performance. Adapted from (Dickinson et al., 2000).

and Rome, 1994). However, if muscles are stretched due to external forces, they act as brakes, dissipating energy. For example, in the running cockroach, the leg extensor muscle 179 produces a larger force while lengthening as compared to shortening (Ahn and Full, 2002) – dissipating more energy than it produces. Finally, *in vivo* measurements of hopping wallabies (Biewener et al., 1998), running turkeys (Gabaldon et al., 2004) and running guinea fowl (Daley and Biewener, 2003) reveal that muscle fibers are near isometric, while spring-like tendons stretch and shorten. In these examples, the muscle acts as struts, facilitating the storage and release of energy in the elastic tendon during locomotion to improve efficiency. The intrinsic properties of muscle, the mechanical properties that depend on length, velocity, and activation, play an important role in energy management during locomotion.

Mechanical feedback is sufficient to alter the function of muscle without any changes in the neural activation. In this research, we determine how the fundamental properties of muscle dynamically interact to form a variety of emergent behaviors during movements with just mechanical feedback.

## A Three-Element Muscle Model Captures the Fundamental Properties of Muscle

Hill's viscoelastic muscle model effectively and accurately captures the salient mechanical properties of muscle (Gasser and Hill, 1924). This three-element phenomenological model consists of (1) a contractile element (CE) with activation dependent viscous properties, (2) a parallel elastic element that acts in parallel to the viscous element, and (3) a series elastic element (SEE) that acts in series to the other

elements.

Among other situations, the three-element model can explain the time course of muscle force development during isometric activation, and changes in force due to muscle shortening (Katz, 1939). Upon activation, the force produced by a muscle develops asymptotically towards a steady-state value. Applying the viscoelastic analysis, the rate of force development can be explained by the graduate internal shortening of the active viscous element that stretches the series elastic element. During a quick-release, a rapid shortening of an initially active isometric muscle, the force rapidly drops before asymptotically increasing again towards its initial isometric force. The initial drop in force is due the rapid shortening of the series elastic element, but not the viscous element. The slow redevelopment of force is due to the shortening of the active viscous element, stretching the series elastic element. The viscoelastic model explains a variety of muscle functions.

Although this model does not give insight into the molecular mechanisms in muscle, it provides a computationally efficient and resonably accurate representation of the mechanical properties of muscle. Further, the viscoelastic model has greatly influenced our study of muscle function during movements. A mathematical description of the three-element model is provided in Chapter 3.

## Contractile Mechanisms and the Fundamental Mechanical Properties of Muscle

The organization and function of the anatomical components of muscle gives rise to its unique mechanical properties. A muscle fiber is comprised, in part, of myofibrils that are

further constructed of chains of sarcomeres. Each sarcomere contains the contractile proteins that are responsible for force generation. Huxley's Sliding Filament Theory, still widely accepted today, explains how the different components of the sarcomeres function to create force and contraction (Huxley, 1957). Muscle contraction results from the sliding of filaments—protein structures in sarcomeres —over each other. During contraction, the heads of the thick myosin filament attach to binding sites on thin actin filaments, to create links, apply a force, and rotate. The rotation causes the actin filament to move and slide over the myosin filament allowing the muscle to shorten. At the end of the rotation, the myosin heads detach from the actin filament, return to their original state, and bind to a new site to continue shortening. The force generated by the muscle is proportional to the number of attached binding sites.

The anatomical components of muscle can be loosely mapped to Hill's three-element muscle model.

**Contractile Element**

The CE is the active force-producing component consisting of cross-bridge machinery. The forces produced by the CE are subject to length and velocity dependencies.

The maximum force that a muscle can produce depends on the length of muscle (Gordon et al., 1966) ( active force–length relationship). At long lengths, the actin and myosin filaments do not overlap. As a result, during muscle activation at long lengths no actin-myosin links can be created and thus no active force is developed. At intermediate lengths, the overlap between actin and myosin filaments increases the number of binding

sites, and increases the ability of the muscle to produce active force. At very short lengths, the actin filaments from one side of the muscle begin to overlap with the other side (double overlap), blocking potential binding sites, and reducing the muscle's ability to produce active force.

The maximum active force that a muscle can produce also depends on the velocity of muscle (Hill, 1938) (force–velocity relationship). Hill's thermodynamic experiments revealed a relationship between the rate at which heat was released from the muscle and the load applied to the muscle during shortening. Examined differently, his experiments articulated that the maximum active force a muscle could produce was inversely related to the speed of contraction. With increased speeds of shortening, the myosin heads spend more time in states where they are detaching and attaching and do not generate forces. When the muscle is active and legthening, however, the myosin heads are continually stretched past the initial length where they typically bind to the actin filament and spend less time in a detached state. As a result, the maximum active force a muscle can produce increases with the rate of lengthening.

**Parallel Elastic Elements**

Passive elements, such as titin, act in parallel to the CE and contribute to the force a muscle can produce. Increasing the muscle length, and stretching these elements, increases the passive force the muscle produces (passive force–length relationship). These parallel elastic elements act in parallel to the active CE, and therefore, the total force the muscle can produce is the sum of the force produced by the two elements.

### Series Elastic Elements

The contractile and parallel elastic elements in muscle exert their force on the body via SEEs such as the tendon, aponeurosis, and intramuscular elements (Roberts, 2002). Although SEEs are distributed throughout the muscle, the Hill's three-element model lumps them into single elastic element. SEEs stretch proportionally with force decoupling the kinematics of the CE from the body. Typically, a maximal isometric contraction of the muscle can stretch SEEs by 10 to 20% of the entire muscle length. As a result, SEEs may allow muscles to function outside the limitations of the cross-bridge dynamics (force–length and force–velocity relationship) and improve performance during movements. SEEs also have the capability to store and release energy, which has important implications in muscle performance and efficiency during locomotion.

## Isotonic Power Production

Hill's three-element model has shaped our initial understanding of muscle function in behaving animals. The force–velocity property of muscle has especially been used to analyze the energetic properties of muscle during locomotion. In this research, however, we show that a variety of the fundamental properties of muscle work synergistically to enhance muscular performance. This section provides examples on how the force–velocity property has been used to analyze muscle performance and then motivates the need for more complete examination of muscle function.

In order to measure the force–velocity relationship property of muscle, isotonic (constant) loads are applied to a contracting muscle. During an isotonic contraction, the muscle shortens at constant speed and produces a constant force. Because the force is constant,

the SEEs are not changing lengths, and the force–velocity relationship of the CE can be measured at specific muscle length. The force–velocity property of muscle also predicts the maximum rate at which a muscle can produce mechanical energy or work (Josephson, 1993).

Isotonic contractions have also been used to approximate the energetics of muscles during movements. Power, the rate of work production, is defined as the product of the shortening velocity and the muscle force. Therefore a muscle can only produce power when it is both producing a force and shortening. Power generation is zero at the maximum shortening velocity ($v_{max}$) where the muscle is unable to produce a force and at zero velocity where the force is maximal but no shortening is occurring. For a range of velocities (approximately 0.2 $v_{max}$ to 0.4 $v_{max}$), power generation is maximal. Muscle power generation also depends on muscle length and muscle activation which affects the force the muscle is generating (Josephson, 1999).

Several studies have suggested that, during locomotion, muscles shorten at velocities where it can produce a maximum amount of power. For example, in the swimming scup (Rome et al., 1992) and carp (Rome and Sosnicki, 1990), the red muscles shorten at velocities where maximum power is generated, independent of temperature (Rome et al., 1992). At higher temperatures, the maximum shortening speed ($V_{max}$) of the red muscles increases but the muscle still operates at velocities where maximum power is generated. As a result, in warmer temperatures, the scup is able to swim significantly faster. In the carp, Rome showed that the red and white muscle fibers operate at velocities that produce maximum power (Rome et al., 1988). At slow swim speeds only the red muscle fibers

are recruited. During a startle response, where the swim speed is high, it would be impossible for red muscles alone to generate enough power; the muscle would have to shorten at velocities greater than their $V_{max}$. During this quick escape swim, red and white muscle fibers are recruited. White fibers have a greater $V_{max}$ and both muscles operate at velocities that generate maximum power. By changing gear ratios, gait, or using a variety of muscle the neuromuscular system may insure that muscles shorten at velocities where maximum power can be generated.

Unlike the early assumptions of the isokinetic movements, muscle must accelerate and decelerate and therefore operate over a range of velocities during locomotion. Lutz and Rome have suggested that frog SM is designed to produce peak power during jumping (Lutz and Rome, 1994). Their *in vivo* measurements of the SM during jumping have shown that it shortens (1) at a constant velocity where peak power is generated (Lutz and Rome, 1996b), (2) over a range of sarcomere lengths where maximum force is generated (Lutz and Rome, 1996a), and that (3) the muscle is maximally activated during the jump (Hirano and Rome, 1984). However, some of these results do not consider the dynamics involved in maximizing a jump. A constant shortening velocity is achieved when the muscle is working against a constant antagonistic load that does not include inertia - which is not similar to that expected during jumping.

The velocity of the frog body increases, and is not constant, throughout the contact phase of a jump (Roberts and Marsh, 2003). Lutz and Rome calculated the velocity of shortening in the SM by estimating the hip and knee joint angles from film acquired from a high-speed camera. Because the SM moment arm at the hip is constant and relatively

small at the knee (Lutz and Rome, 1996a), if the SM shortens at a constant velocity the frog body must also be shortening a constant velocity. Such a movement requires a large initial acceleration and is inefficient. Even if the duration of acceleration is short and the body can quickly reach its peak velocity, the frog's muscles should stop producing force because any energy expended by the muscle after this point is wasted except to raise center of mass before take off. To maximize efficiency, the frog body should reach peak velocity and full extension at the point of take off. In Chapter 3, we examine how the elastic and contractile elements in frog SM can improve power production during jumping. We employ a more realistic mechanical context for jumping, and investigate the SM as it accelerates an inertial load.

## Muscle Energetics During Cyclical Movements

In order to more accurately replicate the function of muscles during locomotion, muscle energetics are typically studied in cyclical movements called work loops (Josephson, 1985). During most types of locomotion the joints in the limb undergo cyclic changes in angle causing the muscles that span the joints to continuously lengthen and shorten. If the muscle is active and producing a force during shortening it is performing work and facilitating the movement. If the muscle is producing a force during lengthening, it is resisting the movement, and absorbing work. During a cycle, the work generated or absorbed by the muscle can be calculated by measuring the area enclosed when plotting muscle force against muscle length (positive is shortening) forming a work loop. Parameterized in time, if the loop is traversed clockwise the work is negative and mechanical energy is dissipated. Traveling counter clockwise indicates that work is generated.

Although the work loop method facilitates the study of muscle under specific circumstances, the muscle cannot be examined under natural conditions where it interacts with other mechanical structures in the environment. Traditionally work loops prescribe the length trajectory of the muscle (usually a sinusoid) regardless of the force the muscle is producing. As a result, the interactions between the mechanical properties of muscle and external forces cannot be investigated. Recently closed-loop experimental techniques have been developed that couple an isolated muscle with a computational load (Farahat and Herr, 2005; Lin and Rymer, 1998). These systems enable the study of real muscle tissue during dynamic tasks where previous studies were constrained to using muscle models for such investigations. In this dissertation, we examine the mechanical properties of muscle using a closed-loop system. In addition, we extend current closed-loop methods, enabling an isolated muscle to interact with physical loads. Physical loads, as apposed to computational ones, can be more complex and better represent the natural loads muscles work against *in vivo*.

## Stability

Animals have the remarkable ability to maintain balance and easily traverse a variety of uneven terrains. During locomotion, animals use their muscles to interact with complex environments and work against a variety of loads (Marsh, 1999). The interactions between the musculoskeletal plant and environment are dynamic and change with the speed of locomotion, the type of locomotion, and physical disturbances in the environment. As a result, the neuromuscular system must continually stabilize the animal.

During rapid movements, the mechanical properties of muscle may play important roles in maintaining stability. Unlike sensory feedback, which is subject to time delays, the intrinsic properties of muscle react instantly to mechanical feedback and can immediately mitigate mechanical perturbations. In Chapter 4, we investigate the ability of the mechanical properties of muscle to maintain a dynamic stable bouncing gait.

Dynamic stability is a measure of the ability of the system's state variables (position, velocity, etc.) to maintain to a steady-state periodic gait (Full et al., 2002). During a periodic gait, the state variables temporally oscillate from step to step. Parameterizing the state variables as function of time and plotting the relationships between the states (i.e. position vs. velocity) provides a limit cycle. A periodic motion results in a closed-loop limit cycle. The limit cycle is considered to be stable if other paths, which may arise from perturbations, converge back to the limit cycle. The study of dynamical systems has provided several tools to determine if limit cycles are stable and how fast the other paths converge on to the limit cycle. In this dissertation, we employ a return map analysis to quantify dynamic stability. The return map examines the dependency of one state variable (i.e. velocity), at particular moment in the gait (i.e. position = 0), on the same variable at the same moment in the gait during the previous period or step (Seyfarth et al., 2003). More details about the return map analysis can be found in Chapter 4.

Computational and experimental methods are used, often separately, to study how muscles can stabilize a limb. Computational models allow measurements of the neuromuscular system, during complicated but controlled conditions, which are not accessible with experimental methods. However, computational models are limited by

our current understanding of each of the components that comprise the model. While experimental methods allow the actual neuromuscular system to be examined, obtaining accurate data during controlled conditions is difficult. In this research, we combine computational approaches with isolate muscle experiments and yield novel information about the function of and the mechanical properties of muscle.

## Frog Model

Due to a wealth of previously published data, we use the isolated frog hindlimb muscle to test our hypotheses throughout this dissertation. Historically the frog has been used to study the basic physical properties of muscle, the role of spinal pathways, and locomotion strategies—spanning the entire hierarchy of the neuromuscular system. Early force–velocity and force–length experiments were conducted with frog muscle tissue (Close, 1972; Hill, 1938; Julian et al., 1986). Frog extensor muscles are also used to study the energy generating capabilities of muscle (Ahn et al., 2003; Lutz and Rome, 1996b). The energy protocols typically involve activating the muscle while forcing it through a specific length trajectory. Frog muscle models have been developed to study particular muscles as they interact with simulated mechanical systems (Kargo and Rome, 2002; Roberts and Marsh, 2003; Shadmehr and Arbib, 1992). The kinematics and activity of the hindlimb have been thoroughly studied in swimming and jumping in a variety of frog and toad species (Rana pipiens - (Hirano and Rome, 1984; Johansson and Lauder, 2004; Kamel et al., 1996; Lutz and Rome, 1994; Peters et al., 1996), Rana catesbeiana - (Olson and Marsh, 1998; Roberts and Marsh, 2003), Rana esculenta - (Nauwelaerts and Aerts, 2003; Nauwelaerts and Aerts, 2006; Nauwelaerts et al., 2005), Bufo marinus - (Gillis, 2007; Gillis and Biewener, 2000)) . Kinematic markers have been used to identify and

compare joint angles and muscle lengths during in vivo jumping and swimming. Electromyograph recordings are also obtained to determine the activity of different muscles and illuminate the strategies that the frog neuromuscular system uses to efficiently generate power and locomote. A large body of literature on the frog neuromuscular system exists to build our studies upon.

## Potential Applications

The development of biologically inspired neural prosthetics relies on a suitable mechanical actuator to produce life-like movements. Investigating muscle tissue may give rise to a design for an efficient mechanical actuator that exhibits the required dynamics. Current biomimetic actuator technology (Caldwell et al., 1995) has not been able to replicate the energetics, and robustness of muscles (Caldwell and Tsagarakis, 2002). Muscle tissue is considered to be 40-75% efficient and has the ability to repair itself. The viscoelastic properties of muscles help give rise to natural movement (Pratt, 2000) and actuator efficiency (Meijer et al., 2003). In contrast to artificial actuators, muscles consume a renewable resource while producing environmentally friendly waste (Caldwell and Tsagarakis, 2002; Herr et al., 2001). Some researchers argue that using real muscles or developing true artificial muscle actuators will propel prosthesis design (Meijer et al., 2003).

Robotic systems are severely limited in their ability to negotiate unknown terrains. While most current robots are used in manufacturing environments, where the entire physical environment is meticulously specified, the long-term goal of robotics is to build autonomous systems that can interact with humans and negotiate unknown environments.

Trajectory controlled robotic systems rigidly specify the position of each joint. Unlike biological systems, trajectory controlled robots are energetically inefficient and struggle to locomote in unspecified environments. Recently, robotic systems that are inspired by the biological systems have begun to consider the role of the neuromuscular system. For example, RHex, a hexapod robot that mimics some the mechanical properties of the cockroach leg, is able travel over a variety of unknown terrains at speeds greater than one body length per second (Altendorfer et al., 2001). RHex's unparalleled performance emerges from its biologically inspired sprawled posture, passive compliance, and gait. Still, substantial research on the basic properties of the neuromuscular system needs to be completed to develop more complex robotic systems that can serve a variety of purposes.

For patients with certain neurological disorders including spinal cord injury and stroke, delivering electrical current pulses to the nerves that innervate the paralyzed muscles can elicit contractions (Peckham and Knutson, 2005). Currently, most clinically available functional electrical stimulation (FES) systems are open-loop (for review see (Peckham and Knutson, 2005) , (Loeb and Davoodi, 2005) and (Popovic et al., 2001)) and thus cannot stabilize mechanical perturbations well. FES works by depolarizing the motor neuron, triggering an action potential that crosses the neuromuscular junction and evokes contraction (Peckham and Knutson, 2005). Though FES systems hope to one day help patients walk (Johnston et al., 2003), the most common uses today for FES as neural prostheses, include drop foot (where the foot drags along the ground during the swing phase of walking) (Lyons et al., 2002) and hand grasping (Popovic, 2003). Freehand®, the first FDA approved FES system for hand grasping (Popovic et al., 2001), uses the patient's contralateral shoulder position to determine the hand-grasp position (Peckham

and Knutson, 2005). The recently developed BIONic WalkAide, using an injectable stimulator called the BION (Cameron et al., 1997) to stimulate the deep peroneal nerve, uses a simple tilt sensor to correct drop foot (Weber et al., 2005; Wieler et al., 1999). Improving current FES tecniques and prostheses requires the use of closed-loop paradigms that can react to the environment using strategies similar to those used by an intact neuromuscular system.

Using closed-loop paradigms, which make use of feedback to modulate the electrical stimulation patterns, it is possible to effectively control the force generated in paralyzed muscle (Chizeck et al., 1988; Chizeck et al., 1991; Crago et al., 1980a). These paradigms, however, do not infer what force the neuromuscular system would normally produce. For example, a feedback controller that maintains a constant stiffness was recently developed (Crago et al., 1991; Lan et al., 1991; Lemay et al., 1993). A controller that maintains constant stiffness may not allow the patient to utilize the intrinsic stabilizing properties of muscle. As such, the resulting motions may be unnecessarily stiff and the controller may needlessly fatigue the muscle. Investigating the dynamics of the neuromuscular system may help us design efficient controllers for prosthetic systems.

## Summary

Muscles interact with the physical environment and function in a variety of ways to manage mechanical energy. During locomotion muscles produce, absorb, and dissipate energy to successfully propel and stabilize the body. In this thesis, we examine how series elastic and contractile elements in muscle function together to maximize power

production and stabilize perturbations during locomotion using a closed-loop system.

In Chapter 3, we hypothesize that SEEs can function to temporally concentrate energy transfer from the CE to the body and enhance power production during a jump. SEEs, which are not limited by crossbridge dynamics, can stretch and shorten to store and release energy respectively. We analyze the kinematics and energetics of a single muscle working to accelerate an interial load using three different strategies to transfer energy to and from the SEEs.

In Chapter 4, we hypothesize that the intrinsic properties of muscles, without sensory feedback, can stabilize a bouncing gait. Perturbation responses based on sensory information are subject to time delays restricting their stabilizing abilities. The intrinsic properties of muscle, however, can respond to perturbations instantly, changing the force produced when muscle length is altered. We examine the kinematics and energetics of a single muscle in the stance phase of a simple bouncing gait model.

To test our hypotheses, we first (Chapter 2) developed a closed-loop system that enabled us to examine the kinematics and energetics of an isolated muscle while working against complex loads. In addition, we compared our results to those produced Hill-style muscle model performing the same tasks. By combining experimental and computational techniques we can comprehensively test our hypotheses and separate the function of the CE and SEEs.

# CHAPTER 2

# CLOSED-LOOP COUPLING OF A MUSCLE TO A ROBOTIC DEVICE FOR DYNAMIC ASSESSMENT OF MUSCLE FUNCTION

## Introduction

Animal locomotion arises from complex nonlinear interactions between the neuromuscular system and its natural environment. Quantifying the mechanical properties of a muscle as it interacts with the environment is essential to understanding the strategies that underlie movement. Muscle function is difficult to quantify in behaving animals because experimental manipulation and measurements of quantities such as force and length are challenging to achieve. In contrast, detached or isolated muscle preparations facilitate controllability and high-resolution data collection but do not replicate the interactions between the muscle and the natural environment. By virtually connecting an isolated muscle to a physical robotic device, we introduce a closed-loop neuromechanical system to study muscle properties during functional dynamic conditions where muscular and environmental forces interact to produce motion.

*In vivo,* muscles act against a variety of complicated and changing loads that are rarely accounted for in isolated muscle experiments (Marsh, 1999; Roberts and Marsh, 2003). Typically, isolated or detached muscle protocols explicitly specify at least one muscle state (length (Gordon et al., 1966; Trinh and Syme, 2007), velocity (Houk et al., 1981; Julian et al., 1986), force (Cavagna and Citterio, 1974; Hill, 1938)) such that it is independent of the other states. For example, single muscle energetics have been

measured using the classical work-loop method in which the muscle length is prescribed to move along a sinusoidal path that is independent of muscle force (Josephson, 1985; Rome and Swank, 1992; Stevens, 1996). Typically, the muscle is stimulated at different phases or for varying duration and the resulting energetics are measured. Such protocols allow muscle properties to be studied under a variety of conditions where particular variables such as muscle length, velocity, or force are controlled well. In such clamped conditions, however, the dynamic interactions between the muscle and its environment are interrupted, so the derived muscle properties may differ from those that might be observed under behavioral conditions.

An alternative approach is to develop closed-loop methods that do not require any muscle states to be explicitly specified, but to arise from realistic dynamic interactions. Recently developed isolated muscle systems use real-time feedback to allow a muscle's force to move a simulated mechanical load (Farahat and Herr, 2005; Lin and Rymer, 2000; Lin and Rymer, 2001). In these systems, the interactions between the muscle and the simulated environment are defined by physical laws of motion such that none of the muscle states have to be predetermined. These approaches are limited, however, by the fact that the complexity of the natural environment is often too difficult to model computationally, especially under real-time constraints.

In cases of complex mechanical dynamics, a physical or robotic model of a system can more realistically simulate the salient dynamics of a system than a computational model. Robots or other mechanical models are often used to create and study the complex interactions that occur during locomotion such as fluid dynamics or ground contact

(Altendorfer et al., 2001; Birch and Dickinson, 2001). For example, during frog swimming, the load on the muscular system is a function of the viscous resistance of the water on the foot and is complicated by the biomechanics of the frog leg. During the power stroke, the webbed toes open to increase resistance and create forward thrust. During recoil, the webbing closes allowing the leg to move through the water without substantially propelling the frog backwards. A physical model of these interactions would provide a realism that a computational model could not.

The purpose of this study was to develop a *closed-loop neuromechanical system* that applies real-time control to couple an isolated muscle to a physical environment using a robotic device. To illustrate the benefits of the neuromechanical system we implemented a simple example of frog swimming. We coupled an isolated frog muscle to a single-degree-of-freedom robotic limb immersed in a tub of water with a real frog foot attached on the end. In addition, we conducted three illustrative experiments to demonstrate how our system enables the precise study of the function of a single muscle during a variety of tasks that would be difficult to reproduce using *in vivo* or isolated muscle techniques. Unlike *in vivo* techniques, we can independently control muscle parameters (i.e. muscle moment arm) and specifically attribute them to changes in muscle function. Such explicit control is prohibitive *in vivo* because of the integrated nature of intact systems, limiting the ability to perform sensitivity and other analyses. The complex interactions between our robotic limb, which includes a biological element, and the environment are difficult to computationally describe preventing current closed-loop isolate muscle systems to accurately replicate them. Further, traditional isolated muscle methods cannot even consider these interactions and would simple force the muscle along a specific trajectory.

Our approach may facilitate better predictions about neuromuscular strategies and muscle function during complex movements.

## System Architecture

The closed-loop neuromechanical system uses real-time feedback to couple an isolated muscle and a robotic device (Figure 2.1). The architecture, implemented on a real-time processor manages a variety of actuators and sensors in a closed-loop paradigm:

1) Electrical stimulation activates the muscle producing a force.
2) The force produced by the muscle is measured and used to specify the torque applied to the robotic device via a torque motor. The robotic device moves and external environmental forces also act on it
3) The resulting position of the robotic device is measured and specifies the desired length of the muscle-tendon unit (MTU) thus closing the loop. A muscle length controller minimizes the difference between the actual and desired muscle length.

### Design Criteria

This implementation of the closed-loop neuromechanical system was built to work with *frog (Rana pipiens*) muscle. To accurately investigate energetics and mechanics of frog muscle, the actuators, and sensors used by the closed-loop system exceeded the required specifications.

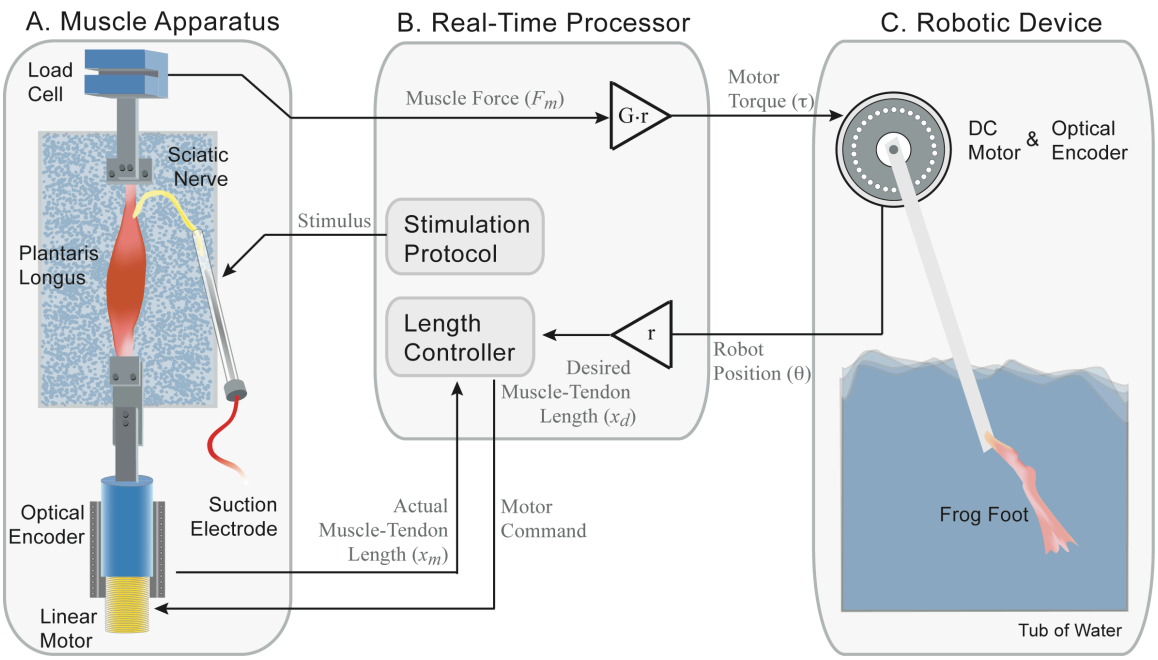


**Figure 2.1: Architecture of the closed-loop neuromechanical system.** An isolated muscle (A) is stimulated and a load cell measures the force. The force is transformed by a virtual mechanical model (in this example, a moment arm transformation) running on the real-time processor (B). The resultant torque is generated by a motor in the robotic device (C). The position of the robotic limb (θ) is transformed into a muscle-tendon length ($x_m$). A closed-loop length controller ensures that difference between the actual muscle length and desired muscle length ($x_d$) is minimal.

Muscle Apparatus

1) A steady-state stiffness greater than 80 kN/m, which corresponds to a strain of no greater than 1% at maximum isometric muscle force for frog muscles (Kargo and Rome, 2002), was required of the muscle length controller.

2) Although most physical systems of interest would have low bandwidths (0-10 Hz), to match the force twitch response of frog muscle a bandwidth of 120 Hz (-3 dB point) is required of the muscle length controller (Farahat and Herr, 2005). Within this bandwidth a relatively flat amplitude response is required such that the controller does not add or remove energy from the system. Changes in

amplitude less than 2 dB were considered appropriate.

3) *In vivo*, the length of muscles in the frog hindlimb can change on the order or millimeters during swimming or jumping (Gillis and Biewener, 2000; Peters et al., 1996). Therefore, a resolution of 10 μm (1% of 1 mm) was required of the muscle position sensor.
4) Typically, forces in the frog hindlimb range from 1 to 15 N (Kargo and Rome, 2002). The muscle force sensor should be able to discern changes in muscle force of as small as 1 mN or less.

Robotic Device

5) The inertia and friction of the torque motor that drives the robotic device were considered to be part of the load. Therefore, we did not require the closed-loop system to account for the dynamics of the torque motor. The electrical time constant associated with the motor and its amplifier are significantly faster than that of the robotic device and not accounted for.
6) Muscle moment arms in the frog hindlimb are on the order of millimeters. Assuming moment arms no greater than 1 cm, the robot position sensor should have a minimum resolution of 1000 ticks per radian. This maps to resolution of 10 μm for the muscle.

**Muscle Apparatus**

We used the isolated frog plantaris longus (PL) to demonstrate the abilities of the neuromechanical system. The mechanical and energetic properties of frog hindlimb

muscles in traditional behavioral and single-muscle preparations are well-known and serve as a good point of comparison (Hill, 1938; Lutz and Rome, 1996b; Peplowski and Marsh, 1997). All surgeries were performed according to procedures approved by the Institutional Animal Care and Use Committee at the Georgia Institute of Technology (Protocol #A04010). Prior to surgery, frogs (*Rana pipiens*) are anestheized with tricaine methanesulfonate (MS-222, 1 g $L^{-1}$). The frogs were then double pithed. The PL, still innervated by its nerve, was removed along with a portion of the sciatic nerve. A bone chip was left at the proximal end and a large piece of tendon is left at the distal end. Small plastic clamps were used to attach the distal tendon to a load cell (Strain Measurement Devices S251) and the proximal bone chip end to a linear actuator (H2W Technologies). The entire muscle was submerged in a bath (22 °C) of oxygenated Ringer solution (NaCl, KCl, $CaCl_2$, $NaHC0_3$).

A suction electrode was used to activate the sciatic nerve and to elicit a force from the muscle. Muscle force ($F_m$) was measured using the load cell. The muscle-tendon length ($x_m$) was controlled using the linear actuator, and the actual muscle-tendon length was measured using a 1 μm resolution optical encoder (Renishaw RGH41X30D05A), exceeding the 10 μm requirement.

**Robotic Device**

To replicate the salient features of frog swimming, we used a single-degree-of-freedom robotic device consisting of a 0.4 cm diameter, 10 cm length aluminium rod with a frog foot attached on the end (Figure 2.2, Table 2.1). The frog foot was cut at the elongated tarsals and rigidly clamped to the device at the tarsometatarsal joint, leaving the webbed

toes intact. The robotic device was then driven by a DC torque motor (Faulhaber 2342-024CR) and moved through a tub of tap water. The limb was designed so that the morphology of the frog foot played the largest role in creating viscous resistance during movement. Torques applied via the DC motor cause the device to rotate, and the position (θ) was measured using an optical encoder (US Digital E3 2500 CPR) which had a resolution of more than 1500 ticks per radian (1000 required). To accelerate the device, the muscle was required to produce enough force to overcome the viscous resistance of the frog foot moving through the water, the inertial forces of the robotic device, gravity, and other nonlinear forces such as friction.

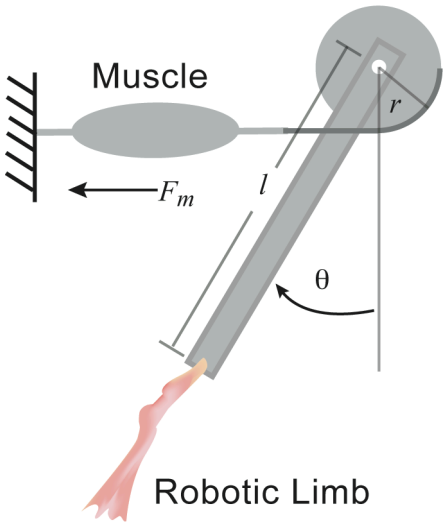


**Figure 2.2: Functional schematic of the closed-loop neuromechanical system.** When the system is assembled it functions as a single joint actuated by a one muscle with a constant moment arm. In this configuration muscle force ($F_m$) causes an increase in joint angle (θ). Gravitational and other environmental forces can act to decrease the joint angle. The force produced by the muscle ($F_m$) is amplified by a gain (G) that is not shown in this schematic.

**Table 2.1: Mechanical Quantities of the Neuromechanical System**

| Symbol | Quantity | Value |
|---|---|---|
| $\theta$ | angle, robotic limb | Output |
| $L$ | length, robotic limb | 15 cm |
| $M$ | mass, robotic limb | 10 g |
| $r$ | length, moment arm | Varied |
| $F_m$ | force, muscle | Output |
| $F_i$ | force, initial muscle-tendon | ~0 N |
| $G$ | gain, force | 3 |
| $x_m$ | length, actual muscle-tendon | Output |
| $x_d$ | length, desired muscle-tendon | Output |
| $x_i$ | length, initial muscle-tendon | Lo* |

* Lo is defined as the length where the muscle-tendon unit can produce the maximum isometric force

## Real-Time Processing

A real-time processor (dSPACE Inc. DS1104) converted the muscle force ($F_m$) to a torque ($\tau$) that was applied to the robotic device using the DC motor. The torque applied to the robotic device was determined by the following equation:

$$\tau = G \cdot (F_m - F_i) \cdot r$$

where $r$ is the virtual moment arm, $G$ is a gain term used to amplify the muscle force. Forces produced by the living muscle were referenced to an initial background force ($F_i$). This allowed the muscle to apply positive and negative changes in force requiring only one muscle to actuate the robotic device in either direction.

Sampled at 10 kHz, the position of the robotic device ($\theta$) was used to determine the muscle-tendon length ($x_m$). The device was connected to the frog muscle via a constant virtual moment arm ($r$). The desired muscle length is computed by the following

equation:

$$x_d = -r \cdot \theta + x_i$$

where $x_i$ is the initial muscle-tendon length. A muscle length controller, running on the processor, minimized the difference between the desired length ($x_d$) and the actual length ($x_m$).

## System Validation

The closed-loop architecture ensured that the virtual connection between the muscle and robotic limb closely resembled a real physical connection. Specifications of the actuators and sensors used by the neuromechanical system exceeded the requirements previously described and are listed in Table 2.2.

**Table 2.2: Muscle Control Specifications**

| Measurement | Quantity | Value |
|---|---|---|
| **Length** | Range | 50 mm |
| | Resolution | 1μm |
| | Bandwidth | 148 Hz |
| | Closed-Loop Steady State Stiffness | 100 kN/m |
| | Gain Margin | > 20 dB |
| | Phase Margin | > 100° |
| | Controller Type | Lead-Lag |
| **Force** | Range | ±20N |
| | Resolution | Analog, 16 bit ADC |

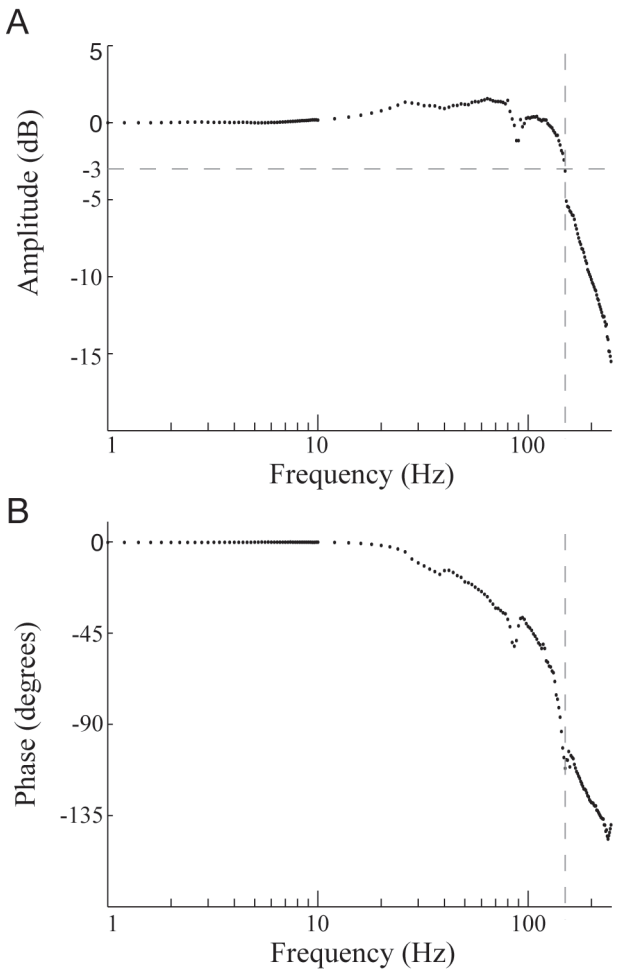


**Figure 2.3: Closed-loop frequency response of the muscle length controller.** The magnitude (A) and phase (B) response of the transfer function was experimentally obtained by sweeping the frequency of the desired muscle length ($x_d$) and measuring the actual muscle length ($x_m$). The reference desired muscle length signals ($x_d$) had an amplitude of 0.02 mm. The -3 dB bandwidth was measured to be 148 Hz and within the majority of the bandwidth (0-120 Hz) changes in the magnitude response were less than ±2 dB.

The muscle length controller was implemented using a second order lead-lag cascade. First, a computational model of the linear actuator was developed and an initial lead-lag controller that met the design criteria was constructed. By trial and error, the initial controller design was tested and modified with the linear actuator in the loop. In

addition, the controller was tested with muscles and springs of various compliances to ensure that controller remained stable. The muscle length controller had a steady-state stiffness of approximately 100 kN/m, surpassing the requirement of 80 kN/m. The frequency response of the controller, without a muscle attached, was experimentally determined by sweeping frequencies with a small amplitude of 0.02 mm (Figure 2.3). The controller was band-limited at approximately 148 Hz (120 Hz required), which was much greater than the natural frequency of our robotic limb. Larger amplitudes saturated the current limit for the muscle length actuator and decreased the bandwidth. During all experiments, the actuator current was monitored to confirm that it was not saturated and that muscle control was not compromised. The muscle length response was relatively flat (within 2 dB) over the entire bandwidth (0 – 120 Hz).

To validate the entire closed-loop system, we compared the torques applied to the robotic device ($\tau$) and the actual muscle length ($x_m$) to their respective desired values during a typical experiment (Figure 2.4). The torques applied to the robotic device (normalized for comparison) accurately matched the forces produced by muscle. The maximum error was $3.3 \times 10^{-5}$ N and therefore, the performance of the entire system is constrained by the dynamics of the muscle length controller. The actual muscle length also accurately matched the desired muscle length ($x_d$) (which is equivalent to the position of the robotic device ($\theta$)). Because forces produced by the muscle acted to displace the linear actuator, the actual muscle length led the desired muscle length when the muscle was producing a force. Due primarily to load applied to actuator by the muscle, and not the dynamics of the lead-lag controller, the maximum error during a typical experiment was 0.12 mm. The virtual connection between the isolated muscle and the robotic device closely

matched a real physical connection.

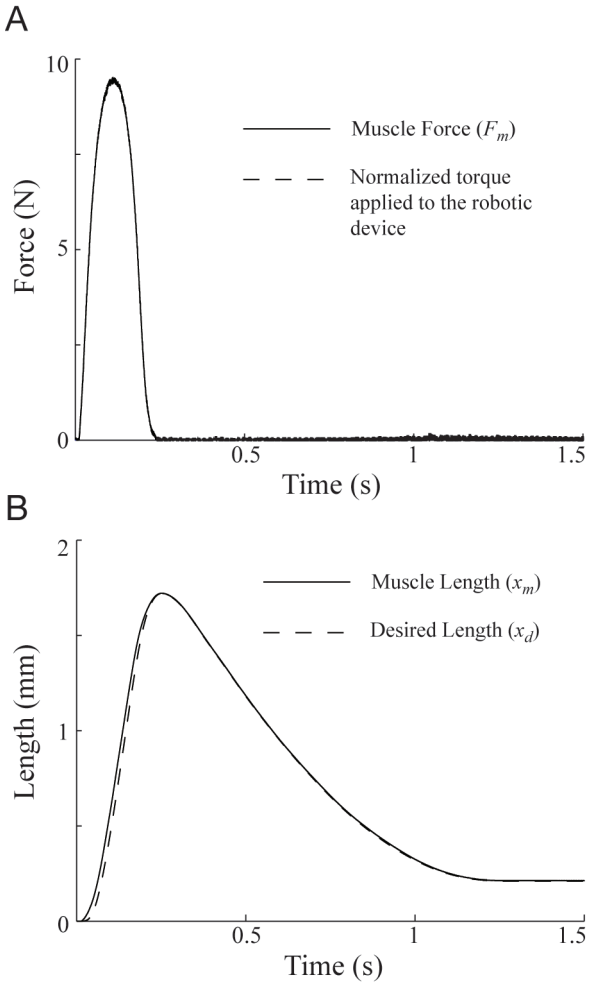


**Figure 2.4: Closed-loop performance of the system during a typical experiment.** (A) The force produced by the muscle ($F_m$) and the normalized torque applied to the robotic device were measured and compared. As desired, the two data sets are indistinguishable validating our ability to accurately apply the forces produced by an isolated muscle to a robotic device. (B) The actual muscle length ($x_m$) closely tracked the desired muscle length ($x_d$). Because of the forces imposed on the linear actuator by the muscle, we found that the actual muscle length ($x_m$) led the desired muscle length ($x_d$). Overall, our closed-loop system performed within the limits of the desired criteria.

## Experimental Design and Results

In order to demonstrate the utility and benefits of the closed-loop neuromechanical system, we conducted three example experiments that varied (1) muscle moment arm, (2) environment viscosity, and (3) muscle fatigue. We show how these variations alter the interactions between the muscle and the environment to affect muscle kinematics and energetics (Figure 2.5, Table 2.3). These examples illustrate how our approach combines the benefits of current *in vitro* and *in vivo* methods.

At the start of each experiment trial, the robotic limb was aligned vertically, and the initial muscle-tendon length ($x_i$) was set to the optimal muscle length $L_o$ (the length where the muscle is able to produce maximum active isometric force), which was determined experimentally from twitch contractions at various lengths. The muscle was maximally activated for 100 ms (approximately equal to the period of muscle activity measured in *Rana pipiens* swimming (Kamel et al., 1996)), and the resultant kinematics were measured. The activation was achieved using a stimulus frequency of 200 Hz and a pulse-width of 100 μs. The stimulus current was adjusted until maximum activation was achieved (1 A). Between each trial the muscle was allowed to rest for two minutes. Isometric contractions were periodically used to check the viability of the muscle. Muscle fatigue was quantified by the percentage drop in isometric force. During the experiments, the muscle was visually inspected, and muscle force recordings were checked to ensure that the muscle did not slip. After data collection was completed, the PL was removed from the bath, all non-muscular tissue was cut away, and the resultant muscle tissue was weighed.

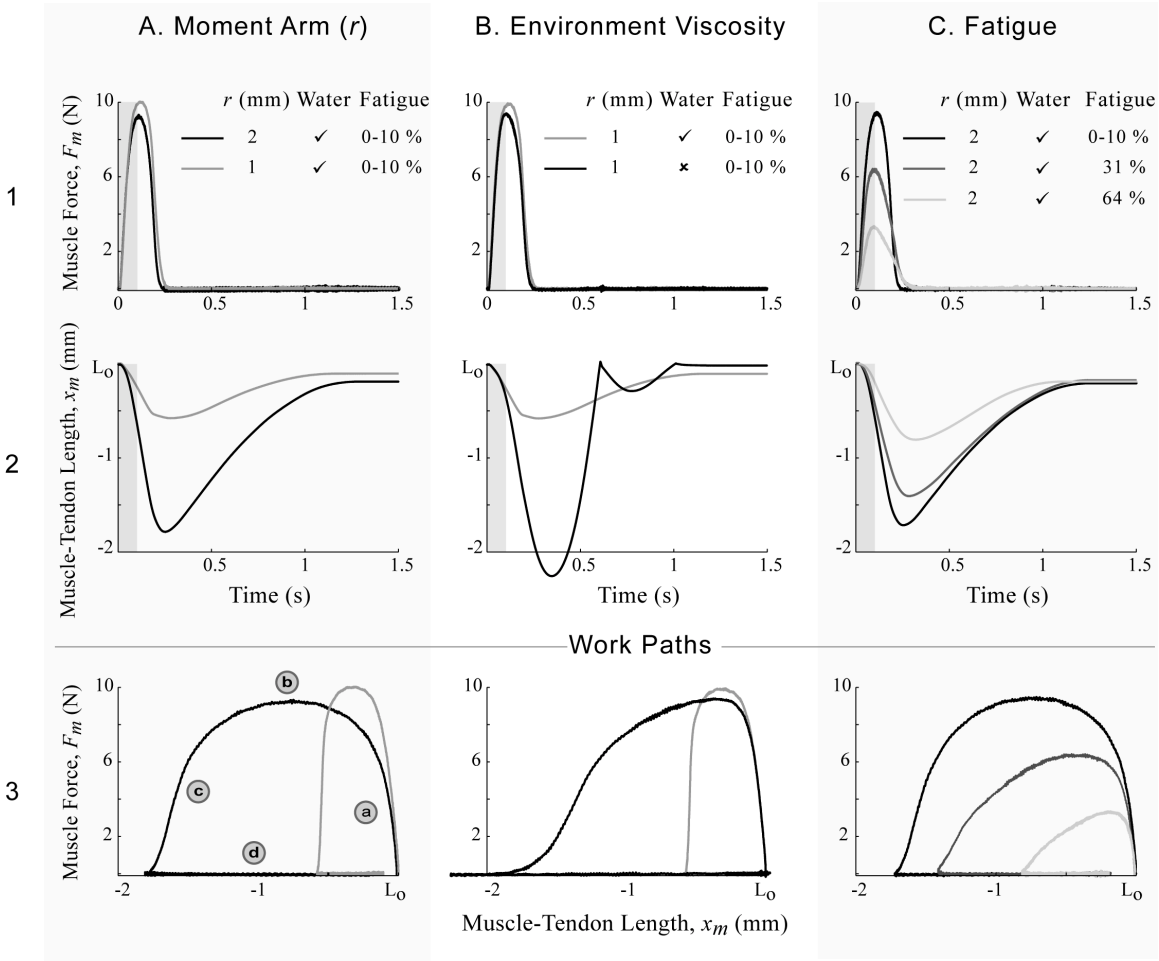


**Figure 2.5: Muscle length and force trajectories.** Each column shows the muscle-tendon length, force, and work-loop trajectories for a variation in one system parameter: (A) muscle moment arm, (B) environmental viscosity, and (C) muscle fatigue. Rows 1 and 2 show the muscle force and length time responses respectively. The duration of muscle stimulation is indicated by the shaded rectangle. The third row plots muscle force versus length to demonstrate the work loop for each experiment. The progression around the work loop is shown in the lower left panel with the following four stages: (a) Upon muscle activation, the muscle force rises without substantial shortening. (b) The power stroke is produced when the muscle shortens while producing a large constant force. (c) After the stimulation is stopped, muscle force declines while inertia causes the muscle to continue to shorten. (d) The muscle passively lengthens due to gravity acting on the robotic device.

**Table 2.3: Muscle Energy and Kinematic Measurements**

| Experiment | Parameters | | | | Values | | | |
|---|---|---|---|---|---|---|---|---|
| | Water | r (mm) | Fatigue (%)* | # Trials | Δ Length (mm) | Peak Force (N) | Work (J/kg) | Avg Power (W/kg)** |
| **Moment Arm** | ✓ | 2 | 0-10 | 3 | -1.72,-1.79,-1.71 | 9.45,9.33,8.67 | 20.0,20.4,17.8 | 81.0,81.1,69.2 |
| | ✓ | 1 | 0-10 | 3 | -0.58,-0.57,-0.57 | 10.03,9.94,9.38 | 7.37,7.24,6.56 | 26.4,26.2,24.4 |
| **Environment Viscosity** | ✓ | 1 | 0-10 | 3 | -0.58,-0.57,-0.57 | 10.03,9.94,9.38 | 7.37,7.24,6.56 | 26.4,26.2,24.4 |
| | × | 1 | 0-10 | 3 | -2.25,-2.28,-2.21 | 9.40,9.29,9.11 | 17.7,17.2,17.2 | 51.5,50.8,51.2 |
| **Fatigue** | ✓ | 2 | 0-10 | 3 | -1.72,-1.79,-1.71 | 9.45,9.33,8.67 | 20.0,20.4,17.8 | 81.0,81.1,69.2 |
| | ✓ | 2 | 14 | 1 | -1.72 | 8.19 | 17.2 | 67.0 |
| | ✓ | 2 | 17 | 1 | -1.72 | 7.86 | 16.6 | 63.3 |
| | ✓ | 2 | 31 | 1 | -1.41 | 6.43 | 10.9 | 37.1 |
| | ✓ | 2 | 48 | 1 | -1.05 | 4.92 | 5.6 | 19.1 |
| | ✓ | 2 | 64 | 1 | -0.81 | 3.35 | 2.9 | 9.2 |

* Fatigue percentage indicates the decline in isometric force.

** Calculated using only the time period during which the muscle is shortening.

The example experiments demonstrate how the neuromechanical system enables the study of muscle kinematics and energetics during tasks that are difficult to study using other methods. For each example, the work-loop technique (Josephson, 1985) was used to measure the work generated by the muscle and to quantify muscular performance. The term work loop typically refers to a particular set of classical experiments where the muscle length is continually oscillated in a predetermined trajectory that is independent of muscle force. While this procedure can replicate the particular trajectory and force combinations measured *in vivo*, it cannot provide information about conditions that deviate from particular situation. Because the causal interactions between force and movement are not considered, the inverse approach of the traditional work look does not allow researchers to study how changes in muscle or environmental properties affect movement and energetics. In our neuromechanical system, the muscle trajectory is not prescribed, but is determined by the dynamic interactions between muscular and environmental forces. Therefore, the forward approach enabled by the closed-loop neuromechanical system allows the causal relationships between a muscle and its environment to vary, thus producing a range of different movement conditions. Although new *in vivo* techniques allow researchers to measure work loops in naturally behaving animals, they are difficult to interpret, as the environmental and muscular forces cannot be independently controlled. While, the interesting dynamic interactions between muscle force, complex environmental loads, and muscle length are maintained (Biewener and Gillis, 1999; Biewener et al., 1998) *in vivo*, change in movement cannot be independently attributed to particular muscular properties as the environment is uncontrolled. Here, by virtually coupling an isolated muscle to a complex load, our system enables the study of

muscle energetics in a manner where the effect of changing different muscular and environmental parameters, such as muscle moment arm, or fluid viscosity, can be assessed in a controlled fashion during causal, dynamic interactions.

**Closed-loop "Swimming" Experiments**

In order to provide a baseline for other experiments, we selected a nominal set of parameters (G = 3, $r$ = 2 mm, water, less than 10% fatigue) that best replicated the *in vivo* kinematics of the PL during frog swimming (Peters et al., 1996). The PL muscle was maximally activated for 100 ms and the force produced was sufficient to drive the robotic limb through the water. The frog foot at the end of the robotic limb opened during limb protraction and closed during limb retraction. During the power stroke the muscle produced a peak force of approximately 9 N (Figure 2.5 A1, black line). This resulted in a peak torque of 0.054 N-m at the robot motor to accelerate the limb. During muscle force production, the muscle shortened at a relatively constant rate (Figure 2.5 A2). Force production ceased at 0.25 s at which point the muscle began to lengthen due to the force of gravity acting on the limb. Because of friction in the motor, the robotic limb did not completely return to its initial position. In the nominal condition, the muscle produced 19 J of work per kilogram of muscle mass, as measured by the area enclosed by the work loop (Figure 2.5 A3). The average power during the shortening phase was 77 W/Kg of muscle mass.

**Varying Moment Arm**

To examine the role that biomechanical configuration can have on muscle work production, we compared two moment arm lengths ($r$): 2 mm (nominal condition) and 1

mm. Reducing the moment arm by one-half resulted in, one third of the work production compared to the nominal condition (Figure 2.5 A, Table 2.3 Biomechanics). Although the peak force produced by the muscle was greater using the shorter moment arm (1 mm), the torque applied to the robotic limb was approximately half of that applied during the nominal condition (2 mm). As a consequence, the robotic limb did not rotate as much through the water using the shorter moment arm. Due to combination of the shorter moment arm and the reduced rotation of the robotic limb, the muscle shortened at slower speed during the power stroke compared to the nominal condition. The decrease in work production using the shorter moment arm was primarily due to the 67% decrease in muscle length excursion.

**Varying Environment Viscosity**

To illustrate how environmental viscosity can affect muscle work production, we allowed the robotic limb to rotate through air instead of water. A 1 mm moment arm was used because the nominal moment arm (2 mm) caused the robotic limb to rotate 360°. The work and average power generated by the muscle doubled when the limb rotated through air (Figure 2.5 B, Table 2.3 Environment) when compared to water. Although peak muscle force was similar in both conditions, total limb excursion was 3 times greater because of the decreased viscous resistance of air. In contrast to the other conditions, the muscle continued to shorten even after the muscle stopped producing a force. During protraction, the robotic device bounced off the mechanical stopper (indicated by the discontinuity in muscle length trajectory, Figure 2,5 B2). The area enclosed by the work loop was 2.5 times greater when the viscosity of the environment was reduced.

### Effects of Fatigue

To study the effects of fatigue, we examined the force and work produced by fatigued muscles under the dynamic loading conditions; here our methods differ significantly from traditional work-loop approaches where the muscle length may be constrained to a nominal trajectory as muscle force decreases. We measure fatigue as the drop in muscle isometric force. With increasing muscle fatigue, the peak force produced and total length shortened during the power stroke declined (Figure 2.5 C, Table 2.3 Fatigue). As peak force declined, less torque was applied to the robotic limb, causing both the total muscle excursion and the speed of shortening to decline (Figure 2.5 C2). While decreased torque contributed to the decline in work production, the reduced speed of shortening further reduced work production, as evidenced by work loops that were triangular rather than rectangular in shape. For example at 48% fatigue (the isometric force generating capabilities of the muscle have dropped 48%), the work (force x length) produced declined by 71% and average power was reduced by 75%

## Discussion

We developed a closed-loop neuromechanical system that facilitates he study of interactions between an isolated muscle and environmental loads via a robotic device. Improving upon previous methods, which were limited to simple computational loads (Farahat and Herr, 2005; Lin and Rymer, 2000), our system enables muscle kinematics and energetics to be studied under a variety of complex physical loads in a controlled manner that better mimics natural behavioral conditions. We were able to study a muscle interacting with the complex fluid dynamics of a frog foot in water, which could not have

been accurately simulated computationally. The closed-loop neuromechanical system has the potential to improve our understanding of the dynamic interactions between a muscle and its environment that underlie natural movements, and could serve as a platform to test functional electrical stimulation (FES) methods for rehabilitation of movement.

We used our system to study muscle function in a simplified swimming task. Frog swimming is a complicated locomotor behavior that requires the coordination of multiple extensor and flexor muscles that interact with the environment via the frog foot (Gillis, 2007; Gillis and Biewener, 2000; Johansson and Lauder, 2004; Kamel et al., 1996; Peters et al., 1996). The flexibility, multiple degrees of freedom, and asymmetrical movement of the frog foot create nonlinear hydrodynamics that are difficult to simulate in real-time. By allowing a muscle to interact with a physical environment through a robotic device that includes biological tissue, we can better emulate its natural loading conditions.

Although we have just provided example data, our results suggest that the neuromechanical system can be used investigate muscles and their function under behaviorally-relevant dynamic conditions. The muscle trajectories generated by our system produced features that are comparable to those found during natural frog swimming. In our nominal experimental condition, the change in muscle length was within 10% of that measured in *in vivo* during swimming in frogs; the duration of shortening was also within 20% of that measured *in vivo* (Peters et al., 1996). During synchronous swimming when both hindlimbs move together, the plantaris longus muscle is not typically active during lengthening by antagonistic muscles (Kamel et al., 1996).

Similarly, in all the conditions we tested, the muscle was not active and did not produce any force during the lengthening phase.

Traditional muscle physiology methods were specifically designed to isolate and measure the individual fundamental properties of muscle. These properties are the basis of numerous mathematical models, which are used to predict the function of muscle during complex tasks. However, the emergent behavior of muscle that arises from the interactions of all its mechanical properties cannot be verified experimentally using classical methods.

Our closed-loop system facilitates the systematic, accurate, and behaviorally relevant study of isolated muscle tissue during a variety of situations. Unlike traditional isolated muscle protocols, which predetermine the length trajectory of muscle, our system dynamically couples an isolated muscle to physical load. Using our approach, the muscle length trajectory is not predetermined, but results from the interactions between the forces generated by the muscle, robotic device, and the environment. Recently developed closed-loop isolated muscle systems (Farahat and Herr, 2005; Lin and Rymer, 2000) are also capable producing dynamic force-length relationships that are not prescribed. However, these systems use computational and not robotic devices, limiting their ability to reproduce the complex loads that occur in the natural environment. New *in vivo* techniques enable the study of muscle properties during natural conditions providing dynamic muscle movements and complex environmental loads (Biewener and Gillis, 1999; Biewener et al., 1998). However, like all *in vivo* experiments, accurate control or manipulation of specific system parameters is difficult or impossible to achieve.

In this research, we examined muscle during a power stroke where it starts from rest and then rapidly shortens. We showed how muscle kinematics and energetics were affected by changes in moment arm, environment viscosity, and fatigue. We used these three example experiments to illustrate how our technique builds upon current *in vivo and in vitro* approaches:

Moment Arm - Varying the biomechanical configuration of muscles may help us better understand the functional limits of muscles during movement. Changing the anatomy of muscles *in vivo* is prohibitive. Our method provides researchers with a tool to investigate the effects of musculoskeletal morphology on movement.

Environmental Viscosity – Current closed-loop techniques, which do maintain system dynamics, are still unable to reproduce the complex environmental loads that occur *in vivo*. The neuromechanical system, using a robotic and not a computational device, allows the systematic study of muscle under a variety of complex loads.

Muscle Fatigue - Studying the mechanical properties of fatigued or injured muscle may help develop alternate strategies to improve function of atypical muscle. We illustrated how the hybrid neuromuscular system allows the capabilities and contributions of fatigued muscle to movement to be accurately quantified. These results could not have been obtained using *in vivo* or traditional *in vitro* methods. The controlled and repeatable study of atypical muscle using *in vivo* techniques would be challenging because the quantification of muscle fatigue or injury is difficult. Traditional work loop methods would require a feedforward prediction on how muscle fatigue or injury affects the movement.

Our approach could be extended to more complex experimental motor-control paradigms and robotic systems including those used to examine terrestrial locomotion (Altendorfer et al., 2001) and balance (Scrivens et al., 2008), swimming (Herr and Dennis, 2004), or flying (Birch and Dickinson, 2001). Additionally, the robotic device does not need to be in the same physical location as the muscle apparatus. Through a remote connection it would be possible for the robotic device to be examined in different environments while leaving the muscle apparatus in the lab. The system can also be integrated with a diverse set of experimental test equipment that include different muscles and intact parts of nervous systems. Further, the architecture could be duplicated to include multiple muscles and robotic devices with multiple degrees of freedom.

Our closed-loop neuromechanical approach ultimately has the potential for application in clinical rehabilitation. Current FES research, which is largely concerned with minimizing muscle fatigue and increasing contraction force (Lau et al., 2007; McDonnall et al., 2004; Peckham and Knutson, 2005), may benefit from an improved understanding of fatigued muscle mechanics. Our system could be used to evaluate stimulation techniques (Crago et al., 1980a; Crago et al., 1980b) on muscle—modified by physical injury, neural trauma, or fatigue—during interactions with complex environments. This technology may help advance our understanding of the neuromuscular system and help improve rehabilitation technologies.

# CHAPTER 3

# POWER AMPLIFICATION STRATEGIES IN THE FROG HINDLIMB MUSCLE

## Introduction

Evolutionary pressures have developed extremely effective forms of locomotion, but the optimizations that emerge from the interactions among neural, muscular, and skeletal systems are still poorly understood. The kinematics and physics associated with an isolated jump are relatively simple and make jumping a good system in which to examine these interactions. Frogs, one of nature's best vertebrate jumpers, are believed to exploit elastic elements in muscle to maximize power production during a jump (Marsh and Johnalder, 1994; Peplowski and Marsh, 1997; Roberts and Marsh, 2003). In this study, we demonstrate using both in vitro and computational methods how energy producing and storing elements in skeletal muscle can function together to enhance power production.

Maximizing jump performance requires maximizing power transfer, not just energy transfer, from skeletal muscles to the body. During an isolated jump, forces produced by skeletal muscles accelerate the body from rest to a maximum velocity at takeoff. To maximize the velocity at takeoff, and therefore maximize jump distance, skeletal muscles must transfer large amounts of energy to the body. The acceleration phase, however, is subject to the kinematic limitation of leg length and to the kinetic coupling of length, velocity and acceleration. Therefore, maximizing takeoff velocity, subject to the leg

length limitation, requires maximizing acceleration. As a result, skeletal muscles must maximize power production to maximize jump performance.

The source of power for jumping is the body musculature. Force and power production by those muscles is most often described by a three element, or Hill style, model consisting of passive, elastic elements in series (SEEs) and in parallel (PEE) with an active, contractile element (CE). This description captures both steady state and dynamic performance of musculotendinous actuators under a wide range of conditions (Bobbert, *et al*., 1986 J Biomech 19:887; Sandercock & Heckman, 1997; Siebert, *et al*., 2008). Power is generated by the CE and transferred to the skeletal structure via the passive SEEs, which may also absorb power from the external world, but all muscle power production CE power production is fundamentally limited by cross-bridge kinetic and is inversely related to the speed of shortening (Hill, 1938). As a result, the CE power (the product of force and the speed of shortening) is maximized only over a small range of velocities. Estimates of muscle velocity derived from whole body kinematics suggest that the muscles in frog hindlimb operate at these optimal velocities to maximize CE power production during a jump (Lutz and Rome, 1994; Lutz and Rome, 1996a; Lutz and Rome, 1996b). Energetic analysis of frog jumping suggests that the peak power generated by frogs during a jump is 2 to 8 times the maximum power the CE can produce (Marsh and Johnalder, 1994; Peplowski and Marsh, 1997). To exceed the maximum CE power production either requires another power source within the muscle-tendon unit (MTU) or reveals a failure of the three-element model.

SEEs, which are not limited by cross-bridge dynamics, can act to store and rapidly

release energy (Alexander and Bennet-Clark, 1977). SEEs stretch proportionally with CE force and decouple the CE length from MTU length, allowing the CE to operate at velocities and lengths that differ from that of the MTU. As a result, the SEE facilitates dynamic force production by the MTU to exceed the force-velocity constraint of the isotonic MTU and enhances MTU power production. The interaction between CE and SEE theoretically results in complex transfer of energy between the elements during an isolated jump. Energy is initially stored within the SEEs due to mismatch between force produced by the CE and forces opposing the CE. The opposing force can come from the body inertia, from an antagonist muscle, or from some other external source. During forward movement, the energy stored SEEs is released in addition to the power produced by CE. This allows the agonist MTU to shorten at high velocities where the CE produces little power and force. The extent to which energy stored in the SEE can be released from the MTU during the jump depends on the coordination among CE contracile performance, SEE elasticity.

In this study, we investigate the dynamic interactions between the CE and SEEs during three jump strategies often used by animals. First, we consider a baseline condition where the agonist extensor muscles simply accelerate the body (solo strategy). We then examine the co-contraction strategy where extensors are activated prior to the jump, while antagonistic forces prevent extension. Several small animals use this strategy to store and release energy from SEEs like a catapult (Gronenberg, 1996). Further, *in vivo* measurements suggest that frogs may also use a co-contraction strategy because the extensor muscles in the hindlimb are activated for a substantial amount of time before any extension occurs (Lutz and Rome, 1996b) (Gillis and Biewener, 2000; Kamel et al.,

1996). Finally, we investigate a countermovement strategy where antagonistic forces first lengthen extensor muscles before they shorten and extend the body. The countermovement strategy, used by humans and other larger animals (Anderson and Pandy, 1993) (Alexander and Bennet-Clark, 1977), may help increase the energy transferred from the CE to the SEEs.

We hypothesize that SEEs can function to temporally concentrate energy transfer from the CE to the body and enhance power production during a jump. We employ parallel mathematical simulations and experiments with isolated muscle to examine power flow within the muscle during the three jump strategies. The computational model enabled us to separate the function of the CE and SEEs, which are distributed throughout the muscle and difficult to discern experimentally.

## Methods

We measured the power produced by the (*Rana pipiens*) semimembranosus (SM) as it accelerated an inertial load, simulating its *in vivo* function during a jump. To test our hypothesis, we combined computational and experimental methods to examine the energetics of the frog during the three different jump strategies: (1) Solo, (2) Co-contraction, and (3) Countermovement. Using novel *in vitro* experimental techniques, we first measured the power produced by an isolated SM accelerating an inertial load, simulating its *in vivo* function during a jump. We then used a computational three-element model of the SM performing the same task to estimate energy storage in the SEE.

**Computational Load**

To reflect the role of the SM *in vivo*, we developed a simple computational model of the frog's effective body mass at its hip (Figure 3.1). The frog SM is a biarticular muscle crossing the hip and knee. However, the muscle functions primarily as a hip extensor because the moment arm at the hip is approximately 3-4 mm whereas the moment arm at the knee is about 0.08 mm (Kargo and Rome, 2002; Lutz and Rome, 1996a). The effective load that the SM works against was mathematically represented by the following equations:

$$GF_m r - 9.81 M_g l - F_a = M l^2 \ddot{\theta}$$

$$x_m = r\theta + x_i \qquad (3.1)$$

The load was described as a point mass 30 mm ($l$) away from the center of rotation. This distance is approximately 40% of the snout–vent length in the frogs used. The reflected body mass ($M$) was approximated by scaling the entire mass of the frog by the relative strength (maximum isometric force) of SM compared to other hip extensors (Kargo and Rome, 2002). Therefore, we approximated that one SM carries a load of 14.2% of the entire frog weight. The mass provides the inertial and gravitational load to the SM. For simplicity, we modeled gravity as antagonistic force that always acts perpendicular to the joint and independent of the joint angle (Roberts and Marsh, 2003).

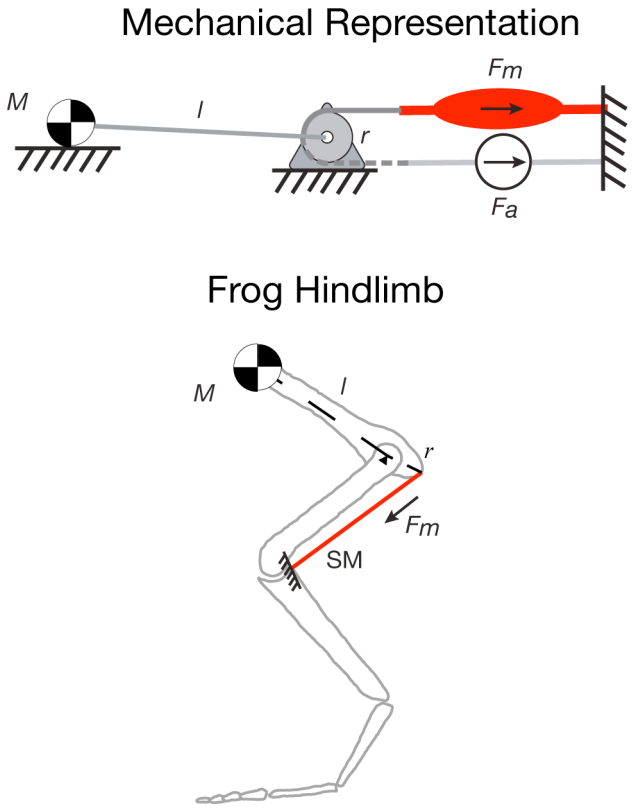


**Figure 3.1: Mechanical representation of the *in vivo* function of the frog semimembranosus.** The SM (red), which has a large moment arm at the hip (*r*) and a negligible one at the knee, produces forces ($F_m$) to extended the hip and accelerate the body during a jump. To replicate its *in vivo* function, we estimated that the SM rotates a portion of the body mass (*M*), represented as a point mass 30 mm (*l*) away from the center of rotation, with a moment arm (*r*). Because of the small moment arm at the knee, we estimated that the distal end of the SM is effectively connected to a mechanical ground. For simplicity, the gravitational weight of the body mass (*M*) always acts perpendicular to the joint angle. Adapted from (Kamel et al., 1996).

The force the SM produces (Fm) acted on the load with a moment arm (r) of 3.5 mm. The muscle force gain term (G) is used to normalize the force in the isolated muscle such that it matched the force in the model. The muscle–tendon length (xm) was determined from the joint position (θ) and was offset by the initial muscle–tendon length (xi) using (Equation 3.1). In experimental trials, muscle force (Fm) was measured from an isolated muscle and applied to the computational load to regulate the length of the isolated

muscle. In simulation trials, muscle force ($F_m$) was estimated from a three-element model, applied to the computational load, and used to regulate the length of the simulated muscle.

**Closed-Loop Experiments**

To determine the energetics of the SM during a jumping task, we used a previously developed closed-loop system that couples an isolated muscle with a variety of complex computational and physical loads. Classic isolated muscle experiments, which simplify the loads applied to the muscle, are not suitable to investigate the role of muscles under natural loading conditions (Marsh, 1999). However, current closed-loop techniques allow an isolated muscle to interact with complex loads (Farahat and Herr, 2005; Lin and Rymer, 2000). This method facilitates the direct measurement of energetics from isolated muscles performing the different jump strategies.

We coupled the isolated frog SM to a computational model of the frog hip, an inertial load. In real-time, the virtual connection between the isolated muscle and computational load was accomplished using the following closed-loop approach:

1) Electrical stimulation activates the muscle producing a force.
2) The force produced by the muscle is measured and used to accelerate the load. Other antagonistic forces can also act on the load.
3) The resulting position of the load is computed and specifies the desired length of the MTU thus closing the loop.

**Experimental Protocol**

All surgeries were performed according to procedures approved by the Institutional Animal Care and Use Committee at the Georgia Institute of Technology (Protocol #A07033). Prior to the surgery, frogs (Rana Pipiens) were anestheized with tricaine methanesulfonate (MS-222, 1 g L-1) and then double pithed. The SM, still innervated by its nerve and attached to bone chips, was removed along with a portion of the sciatic nerve. Small metal clamps were used to attach the proximal bone chip to a load cell and the distal bone chip to a linear actuator. The load cell measured the force the muscle produced and the linear actuator controlled and measured its length. The entire muscle was submerged in a bath (~21 °C) of oxygenated (95% oxygen, 5% carbon dioxide) Ringer's solution (pH 7.1). A suction electrode was used to activate the muscle via the sciatic nerve. For all conditions the muscle was maximally activated (1 mA, 60 Hz, 100 μs).

At the beginning of every experiment the isometric force was determined. The force gain term (G) was used to normalize the isometric force across animals. No other normalizations were applied. Between every trial the isometric force was measured and the gain term (G) was increased to account for fatigue. Between each experimental trial the muscle was allowed to rest for approximately ninety seconds. Isometric contractions were periodically elicited to check the viability of the muscle. Unless otherwise stated, data collection was stopped after the muscle isometric force dropped 10%.

Jump Strategies

We examined the function the SM using three different jump strategies (Figure 3.2). For

each jump strategy, the SM is maximally activated, overcame antagonist forces, accelerated the load, and shortened. The jump was considered complete after the muscle-tendon (MT) length reached a maximal velocity. Any data after this point were disregarded.

Solo Strategy – Only gravitational and inertial loads acted on the muscle. To match the SM's *in vivo* function, we initially stretched the muscle to an initial length ($x_i$) where it is capable of producing 90% of its maximum isometric force (Lutz and Rome, 1994). The muscle is maximally activated for the duration of the jump.

Co-Contraction Strategy – To represent an antagonistic muscle, an idealized antagonistic muscle held the joint in place for 100 ms while the agonist was maximally activated. A virtual ground prevented the antagonist force from flexing the hip further and stretching the SM. The SM was initially stretched to a length ($x_i$) where it is capable of producing 90% of its maximum isometric force. 100 ms after the beginning of the jump the antagonistic force was removed (square edge) and the SM (the agonist) was free to accelerate the load.

Countermovement Strategy – In this strategy, the primary difference was that the antagonistic force was allowed to stretch the SM. The hip started a more flexed position and the virtual ground that prevented the SM from stretching in the co-contraction study was removed. To model the more extended initial position of the hip (which allowed for flexion and a countermovement), initial MT length was set to $L_o$ (the length at which the muscle can produce a maximum isometric force ($F_o$)). Similar to previous conditions the SM was maximally activated at the start of the jump. Typically, the SM took about 8.5

ms to reach the active state and start to produce a force (see Results). As a result, we modeled the same delay for the antagonistic force. During the first 8.5 ms, the antagonistic force held the SM isometric. 8.5 ms after the beginning of the jump, the antagonistic force was applied. The magnitude and duration of the antagonistic force was determined using an optimization process with the muscle model (see next section).

Muscle Characterization

To construct the computational muscle model, several traditional muscle experiments

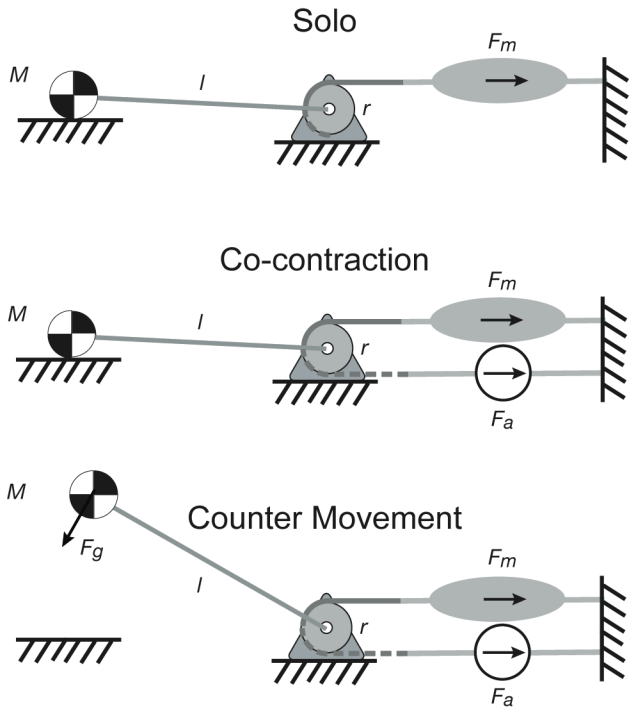


**Figure 3.2: Mechanical model of the effective load for each jump strategy.** For all the strategies, the SM muscle, a hip extensor, acts to rotate a point mass ($M$) with a moment arm ($r$). An idealized antagonistic force ($F_a$) is used for the co-contraction and countermovement jump strategies. For all conditions, the gravitational force always acts perpendicular to the joint. During the solo and co-contraction conditions, the joint rests against a mechanical ground that prevents the muscle from lengthening.

were conducted.

Force–Length – The active and passive force–length (F–L) relationship (Gordon et al., 1966), which describes CE's ability to produce force at different lengths, was determined using 150 ms isometric contractions at pseudo randomly selected lengths spanning 70-115% of optimal length ($L_o$) .

Force–Velocity – The force–velocity (F–V) relationship (Hill, 1938) was measured using a combination of afterloaded ($F_m < 0.7\ F_o$) and isokinetic ($F_m > 0.7\ F_o$) protocols. For all activations, the MTU was stretched beyond $L_o$ such that the time to shorten to $L_o$ was greater than the isometric time to peak tension. For isotonic trials, the muscle was maximally activated and allowed to shorten under force control. The isotonic velocity was determined as the muscle passed through $L_o$. For isokinetic trials, the muscle was maximally activated, and tension allowed to develop isometrically. After the muscle reached a steady-state force the MTU was shortened or stretched using a constant velocity ramp, and force was measured as the MTU length crossed $L_o$. For stretches, the initial MT length was set shorter than $L_o$. Activation duration varied with anticipated velocity but was greater than 150 ms.

Series Elasticity – The series elasticity was measured by rapidly shortening the MTU, which effectively isolates the SEEs. The initial MT length was set at $L_o$ and the muscle was maximally activated. After a steady-state isometric force was achieved, the muscle was subjected to 3 ms shortening at the maximum velocity of the linear actuator. These experiments were completed after the muscle isometric force had dropped between 10%

and 20%.

Activation – The activation kinetics were estimated by measuring the time course of force development during isometric contractions at MT length $L_o$. A least squares optimization process that minimized the differences between the isometric force time course in the model and the averaged muscle response was used to determine the kinetics. During the force development time course, three points of comparison were used: 10%, 50%, and 90% of peak isometric force. For all experimental conditions, the muscle was activated at the beginning of the simulation.

**Computational Muscle Model**

To predict the function of the CE and SEEs, we developed a Hill-type model of the SM. We examined the performance of the model during the three jump strategies. This three-element model, unlike the isolated muscle, has a discrete CE, parallel elastic element (PEE), SEE, which facilitates the study of their individual function.

Muscle force ($F_m$) results from the summation of active and passive components and is transferred to the load via a SEE.

$$F_m = \underbrace{A(t,\tau_1,\tau_2)\cdot f_v(\dot{x}_{ce})\cdot f_{al}(x_{ce})}_{\text{CE active}} + \overbrace{f_{pl}(x_{ce})}^{\text{PEE}} = \underbrace{K_{se}\cdot x_{se}}_{\text{SEE}}$$

The CE force is a function of activation ($A$), CE velocity ( $\dot{x}_{ce}$), and CE length ( $x_{ce}$). The PEE acts in parallel to CE and therefore always has the same length as the CE ( $x_{ce}$).

The PEE force ( $f_{pl}$ ), which is summed along with the CE force to determine muscle force, is a function of its length ( $x_{ce}$ ). The forces produced by the SEE are always equal to the sum of the forces produced by the CE and PEE. The forces produced by the PEE, however, are small and, for the purpose of analysis, considered to be part of the CE force. The total MT length is the sum of the lengths of the CE and SEE ( $x_m = x_{ce} + x_{se}$ ).

To determine the duration and magnitude of the antagonistic force during the countermovement strategy, we used a gradient descent optimization process that minimizes a cost function:

$$Cost = -\frac{\dot{x}_m(t_{off})^2}{t_{off}}$$

The cost function, a measure of jump performance, acted to maximize the square of the takeoff velocity and minimized the takeoff time ($t_{off}$). Minimizing the cost function maximized the average power produced during the jump. The cost function has the same units as power normalized by mass (kg). The magnitude and duration of the antagonistic force was first swept to find initial conditions near the global minimum. The magnitude of the antagonistic force was set to have a limit at $F_o$. The flexors in the frog hindlimb have relatively smaller force producing capabilities as compared to the extensors. Flexor moment arms, however, are larger; therefore, we assumed that flexors and extensors have equal torque generating capabilities.

# Results

In the context of the three jumping strategies described previously, we measured the kinematics and energetics of the frog SM. We combined experimental and computational techniques to examine the power generating capabilities. Our results determine how SEEs function to temporally concentrate energy transfer from the CE to the body and enhance power production during a jump.

## Computational Model

To determine the function of the CE and SEEs, which are not experimentally accessible, we first constructed a Hill-type computational muscle model.

### *Force–Length*

The active ($f_{al}$) and passive ($f_{pl}$) F–L relationships were represented using a third-order polynomial and exponential function respectively ($n$ = 3) (Figure 3.3 A). The mean MT length at $L_o$ was 32.2±1.8 mm (mean±S.D., $n$ = 16) and the SM produced a maximum isometric force ($F_o$) of 4.57±1.8 N ($n$ = 16).

### Force–Velocity

The Hill equation (Hill, 1938) was fitted to the F–V data values ($n$ = 3) between 0.1 and 0.7 $F_o$ and was not constrained to pass through $F_o$ (Figure 3.3 B). The extrapolated maximum shortening velocity ($V_{max}$) was 8.11 muscle lengths per second (ML/s). The extrapolated isometric force was 1.22 $F_o$ (denoted as $F_o$*) and the Hill constant ($a/F_o$*) was 0.28.

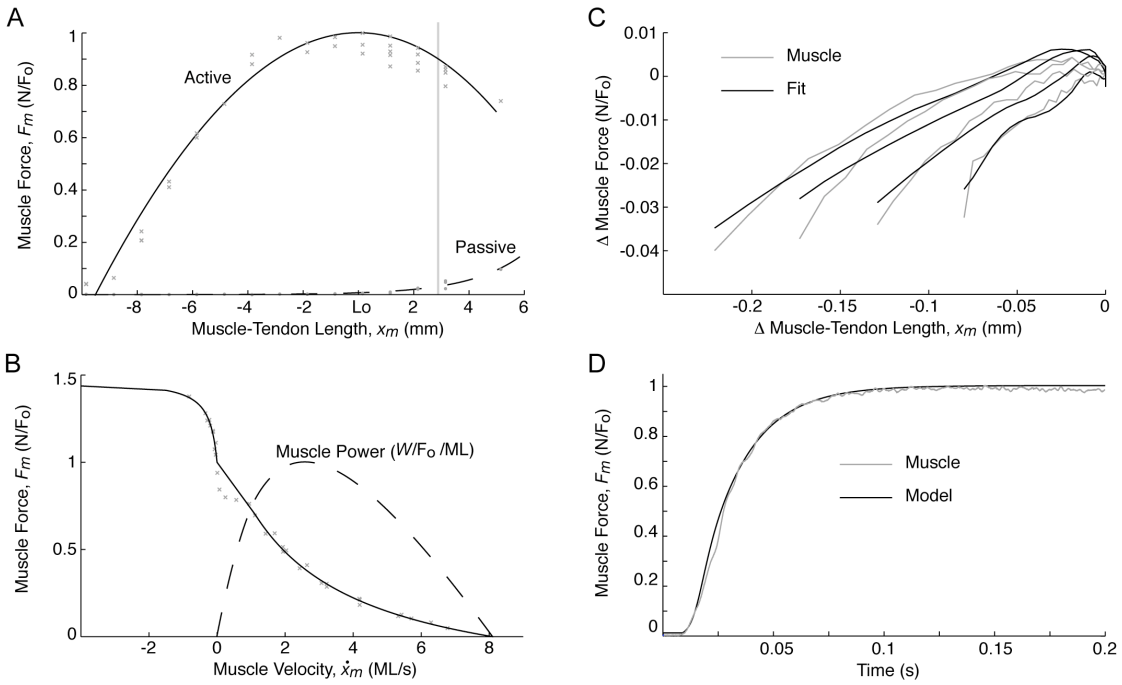


**Figure 3.3: Data and fits used to construct the Hill-style muscle model.** (A) Active and passive muscle force-length properties. Individual data points and the corresponding model estimations are shown. The vertical grey line indicates initial MT length for the solo and co-contraction strategies. The cubic polynomial was scaled such that it passed through a normalized force of 1 at $L_o$. (B) The force-velocity relationship of lengthening and shortening muscle. Individual data points and the continuous fit are shown. The dashed line indicates the normalized power-velocity relationship for shortening muscle. (C) Example series elasticity measurements. Here, the muscle was activated and shortened at different speeds. (D) Comparison of model and an example real muscle force response during an isometric contraction.

For forces between $0.7F_o$ and $F_o$ a linear fit was used (Figure 3.3 B). Although the data were not linear, more accurate fits were not monotonic and resulted in a poor match for the isometric contraction force time course. For lengthening velocities, for which the muscle produces forces greater than $F_o$, the F–V data was fit to an asymptotic function. For velocities greater than 1.5 ML/s the force the muscle produced was relatively constant. A linear approximation with a small slope was used for numerical

implementation reasons.

The following piece-wise, continuous function comprised of the equations described previously represented the F–V relationship over a wide range of operating velocities:

$$f_v(\dot{x}_{ce}) = \begin{Bmatrix} (2.28F_o^* - a\dot{x}_{ce})/(2.28 + \dot{x}_{ce}) & \dot{x}_{ce} \geq f_v^{-1}(0.7F_o) \\ 1 - \dfrac{0.3\dot{x}_{ce}}{f_v^{-1}(0.7F_o)} & 0 \leq \dot{x}_{ce} < f_v^{-1}(0.7F_o) \\ \dfrac{(1.48 - 1)(\dot{x}_{ce}(-357 + 1)) + 1)}{-357 * -0.24} + 1 & -1.5 \leq \dot{x}_{ce} < 0 \\ -0.01(\dot{x}_{ce} + 1.5) + f_v(-1.5) & \dot{x}_{ce} < 1.5 \end{Bmatrix}$$

The power–velocity relationship for shortening muscle was determined from the F–V data (Figure 3.3 B). The muscle is able to produce a maximum power of 1 W/$F_o$/ML or 305 W/Kg at 2.6 ML/s.

Series Elasticity

The series elastic stiffness ($K_{se}$) was measured to be 13.5±2.7 $F_o$/ML ($n$ = 8). The change in muscle force and length, when subjected to rapid shortening, was fitted to a third order differential equation and the elastic term was extracted ($K_{se}$). The velocity of shortening had a small effect on the elastic term in the differential equation (Figure 3.3 C).

Activation

The activation kinematics were described using a sigmoid function:

$$A(t, \tau_1, \tau_2) = \frac{e^{(t-\tau_1)\tau_2}}{1 + e^{(t-\tau_1)\tau_2}}$$

The temporal response of the model force during an isometric contraction closely matched the response of the isolated muscle (Figure 3.3 D). The isometric force time courses in 16 different frogs were characterized at three force time points: $0.1F_o$, $0.5F_o$, and $0.9F_o$. At these forces, the time elapsed was measured: 14.6±1.3 ms, 27.5±2.5 ms, 59±9 ms. Using these force–time pairs, the activation sigmoid time constant ($\tau_2$) and activation offset ($\tau_1$) were calculated to be 570 and 0.017 respectively.

**Experimental Kinematic and Energetic Data**

In all three jump strategies, the isolated muscle produced instantaneous powers that were between 35% and 270% greater than its maximum CE power (Figure 3.4). For each strategy, we measured the muscle force and kinematics from the SM in seven frogs ($n$ = 7). For all strategies, the muscle was maximally activated and the resulting acceleration of the load was measured. Only the mechanical context, or loading condition, was varied between each jump strategy.

During the solo jump strategy, the isolated SM produced a peak instantaneous power that was 35% greater than maximum CE power. Upon maximal activation, the force produced by muscle increased but the MT length remained constant (Figure 3.4 A). After the muscle force was sufficiently large enough to overcome gravity and inertia, the MTU began to shorten. During the early shortening phase, the isolated muscle produced a peak instantaneous power of 1.35±0.11 $W/F_o/ML$, 35% greater than the maximum CE power (Figure 3.4, Table 3.1). The MTU velocity increased throughout the jump until a maximum was reached, denoting the point at which the frog would have left the ground. The MTU reached a peak velocity of 5.56±0.16 ML/s at 84.3±6.5 ms after the onset of

activation. During the contraction, the MTU shortened 8.25±1.04 mm.

For the co-contraction strategy, the addition of the antagonistic force enabled the muscle to produce a peak instantaneous power that was more than twice its maximum CE power (Figure 3.3 B). During the co-contraction period, when the MT length was unable to change, muscle force increased due to activation. After 100 ms, the muscle force approached a steady state level of $0.9F_o$ (as expected based on the prescribed initial length of the MTU). When the antagonistic force was released, the MTU rapidly shortened and produced a peak instantaneous power of 2.37±0.23 $W/F_o/ML$. The MT shortening velocity increased throughout the jump until it reached a peak velocity of 5.78±0.22 ML/s at 153±5.5 ms. If the initial co-contraction time is excluded, the MTU reached a peak velocity in 53 ms. During the contraction the MTU shortened 7.56±0.87 mm.

For the countermovement strategy, the MTU first lengthened before shortening and producing a peak instantaneous power that was greater than the peak power produced using the other two strategies (Figure 3.4 C). The optimal antagonistic force magnitude was limited by the constraints, which clipped the force magnitude at $F_o$. The optimal antagonisitic force duration was calculated to be 17.9 ms after the initial 8.5 ms onset delay. Upon activation, the MTU began to produce force but lengthened due to the antagonistic force. When the antagonistic force was removed, the MTU still continued to lengthen due to inertia. After overcoming inertia, the MTU shortened and produced a peak instantaneous power of 2.71±0.11 $W/F_o/ML$. The MTU reached a peak velocity of 5.98±0.17 ML/s at 91±5 ms. During the contraction the MTU shortened 4.68±0.9 mm.

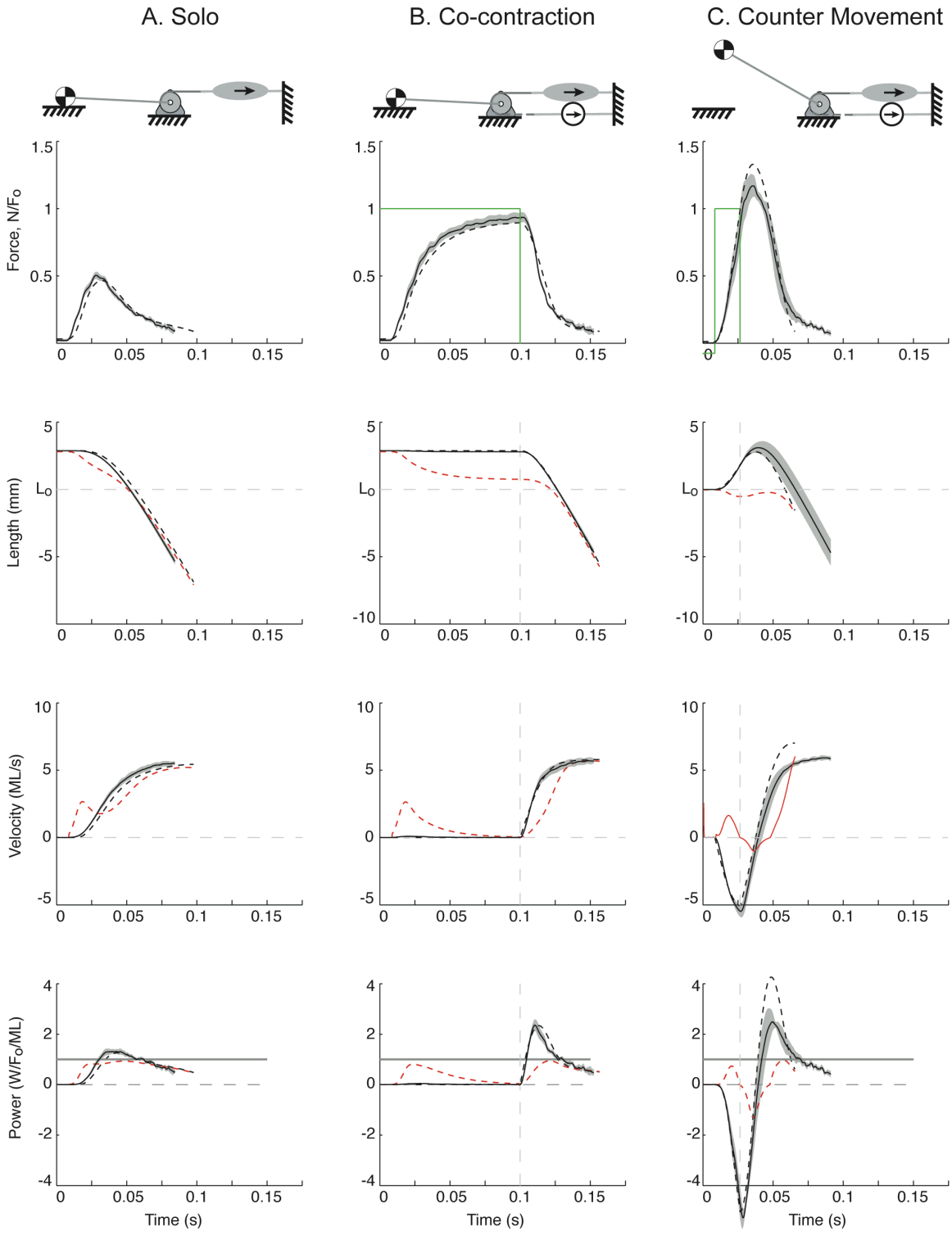
A. Solo
B. Co-contraction
C. Counter Movement
Force, N/Fo
Length (mm)
Lo
Velocity (ML/s)
Power (W/Fo/ML)
Time (s)

**Figure 3.4: Model and experimentally measured muscle kinematics and energetics for each jump strategy.** Each column shows the muscle force, length, velocity and power for a jump strategy: (A) Solo, (B) Co-contraction, (C) Countermovement. In all panels, the trajectories end when the velocity has peaked and the frog would have taken off. The model MT trajectories are shown with a dashed black line and the CE trajectories shown with a dashed red line. The mean experimental MT results are illustrated with a thick black line. The thin black lines indicate the experimental trajectories one standard deviation above and below the mean. Rows 1 and 2 show the muscle force and length time responses respectively. The CE and SEE always produce the same force (assuming that the force produced by the PEE is small). For the co-contraction and countermovement strategies the antagonistic force is shown in green. The length of the SEEs, which is proportional to muscle force, is the difference between the MT (black) and CE (red) length. The horizontal line designates the maximum isotonic power. The vertical dashed line indicates where the antagonistic force stops in the co-contraction and countermovement conditions. Row 3 shows the velocity of the MT and CE. Shortening velocities are positive and lengthening velocities negative. The last row plots the instantaneous power produced by the muscle. For all conditions the instantaneous peak power is greater than the maximum isotonic power.

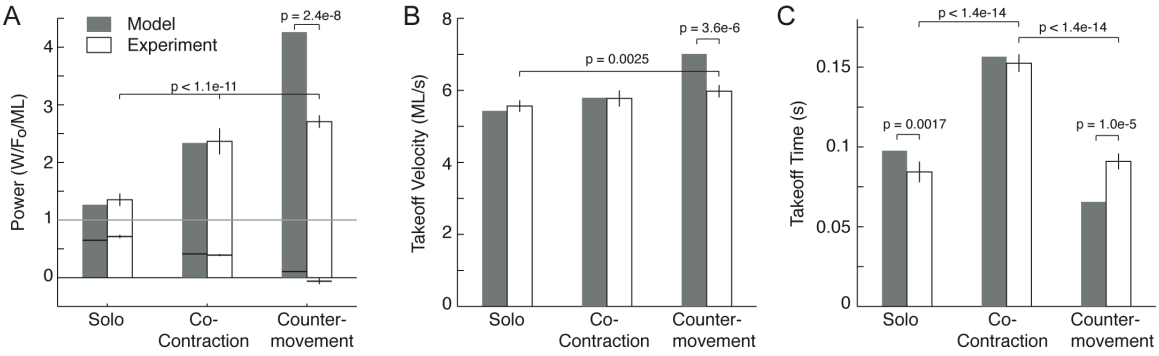


**Figure 3.5: Summary of results for each jump strategy.** (A) Average and peak power produced during the jump. The average power (black lines) is never greater than the maximum isotonic power (indicated by the horizontal grey line). The peak power for all strategies is significantly different that the maximum isotonic strategy ($p < 1.4x10^{-4}$) (B) Takeoff velocities for each jump strategy. (C) Takeoff time for each jump strategy.

**Table 3.1: Summary of Results**

| Strategy | | Peak Power ($W/F_o/ML$) | Average Power ($W/F_o/ML$) | Work ($J/F_o/ML$) | Length Shortened (mm) | Peak Velocity (ML/s) | Takeoff Time (ms) |
|---|---|---|---|---|---|---|---|
| **Solo** | Model | 1.26 | 0.65 | 0.063 | 9.75 | 5.43 | 97.6 |
| | Exp. | 1.35±0.11 | 0.71±0.11* | 0.064±0.004 | 8.25±1.04* | 5.56±0.16 | 84.3±6.5* |
| **Co-contraction** | Model | 2.34 | 0.41 | 0.064 | 8.34 | 5.79 | 156.5 |
| | Exp. | 2.37±0.23 | 0.39±0.02* | 0.065±0.004 | 7.56±0.87* | 5.78±0.22 | 153±5.5 |
| **Counter-movement** | Model | 4.26 | 0.11 | 0.007 | 1.56 | 7.01 | 65.5 |
| | Exp. | 2.71±0.11* | 0.06±0.05* | 0.001±0.005* | 4.68±0.9* | 5.98±0.17* | 91±5.0* |

* Indicates statistical significance between the model and experiment ($p < 0.05$, t-test)
Standard deviations are given after the ±
$n = 7$ for each strategy

**Model Validation**

We compared the muscle force and kinematics measured from the SM in seven frogs ($n$ = 7) with those generated by our muscle model (Figure 3.4). We use this comparison to validate the model, which will facilitate the separation of the individual contributions of the CE and SEEs. To quantify the similarity between the model and experimental data, we used statistical comparison (student t-test) of three primary performance metrics: peak instantaneous power, takeoff velocity, and takeoff time (Figure 3.5). Table 3.1 provides a comparison of several additional kinematic and energetic parameters.

For the solo and co-contraction strategies, the model and isolated muscle data were similar as quantified by their p values and relative error, demonstrating that the model accurately predicted the function of the isolated muscle (Figure 3.4 A and B). As shown in Figure 3.5, the three performance metrics for the solo and co-contraction strategy were not significantly different ($p > 0.05$) from the model prediction except for the takeoff time measured during the solo strategy. The relative errors, however, for all the parameters measured was less than 20% (Table 3.1).

For the countermovement strategy, our three-element muscle model was unable to accurately predict the kinematics and energetics of the isolated muscle. The measured peak power, takeoff velocity, and takeoff time were all significantly different (p values less 0.05) than that predicted by the muscle model. However, during the initial MT lengthening phase of the jump, the isolated and model muscle data are qualitatively similar (Figure 3.4 C). As the MTU continued to lengthen and during the following shortening phase, however, the force predicted by the model was greater than that

measured in the isolated muscle. As a result the kinematics predicted by the model did not match that produced by the isolated muscle. Therefore, we cannot use the model to accurately extract the function of the CE and SEEs in the countermovement strategy.

**Contractile and Series Elastic Element Function**

In all three strategies, the SEEs stored and released energy facilitating the muscle to produce instantaneous powers that were between 35% and 270% greater than its maximum CE power. Combining our experimental and computational results, we showed how energy is stored and released from the SEEs.

For the solo strategy, our data showed that the weight and inertia of the load was sufficient to store energy in the SEEs and to enhance power production. The maximum length of the SEE was 1.03 mm and the length at takeoff was 0.14 mm. This represents a release of 17% of the total work done by the CE. The peak shortening velocity of the SEE was 0.94 ML/s and equates to power release of 0.33 $W/F_o/ML$ or 33% of the maximum power the CE can produce. Initially, when the force produced by the muscle was less than the load, the CE began to shorten while the MT length remained constant (Figure 3.4 A). As a result, the power produced by the CE was stored in the stretched SEEs. This energy transfer from the CE to the SEEs occurred when the power produced by the CE was greater than that power produced by the MTU (Figure 3.4 A, last row). During the shortening phase, the load due to inertia decreased and muscle force declined, shortening the SEEs and facilitating the release of energy previously stored in them. During shortening, the MT velocity was greater than the CE velocity indicating that SEEs were shortening and releasing energy. The transfer of energy from SEEs to the body was

evident when the MT power was greater than the CE power. Both the SEEs and CE shortened and applied power to the body during the shortening phase. As the CE continued to shorten, muscle force declined due to the F–L and F–V properties.

For the co-contraction strategy, the addition of the antagonistic force further facilitated the storage and release of energy in the SEEs (Figure 3.4 B). The maximum length of the SEE was 2.06 mm and the length at takeoff was 0.14 mm. This represents a release of 75% of the total work done by the CE. The peak shortening velocity of the SEE was 2.67 ML/s and equates to power release of 1.4 $W/F_o/ML$ or 140% of the maximum power the CE can produce. During the preparatory co-contraction period, the CE shortened settling to a new steady-state length, stretching and storing energy in the SEEs (CE power is greater than MTU power). When the antagonistic force was released, the MTU rapidly shortened, largely due to the shortening of the SEEs (MT velocity is greater than CE velocity) that released their stored energy in addition to that produced by the CE (MT power is greater than CE power). As the MTU and CE continued to shorten the force declined due to its F–L and F–V properties and the power produced began to decline.

For the countermovement strategy, we could not accurately separate the function of the CE and SEEs. The Hill-type model predicted that CE remained approximately isometric while the SEE stretched and shortened due to the application and removal of antagonistic force respectively.

**Work Loop and Dynamic Force–Velocity Relationship**

We examined the work loops and dynamic force-velocity relationship of the muscle

during the jump (Figure 3.6). Unlike the traditional work loop definition (Josephson, 1985), the MT trajectory in our study was not prescribed but resulted from the interactions between the muscle and the computational load.

Using the solo and co-contraction strategy the muscle initially develops force while the MT length is constant. The CE, however, began to shorten by stretching the SEEs (storing energy). When the muscle force became greater than the load (solo strategy) or the antagonist force was removed (co-contraction strategy), the MTU shortened and the force produced by the muscle declined. The decreased muscle force shortened the SEEs and released the energy previously stored in them. The joint reached a maximal velocity when the muscle force is equal to the load.

For the countermovement strategy, the model predicts a spring-like action for the MTU where the SEEs stretch and shorten like a spring and the muscle dissipates very little energy (Figure 3.6 C). The experimental data, however, did not suggest the same function and a significant amount of work was dissipated. During the lengthening phase, stiffness of the model initially matched the isolated muscle. However, as the muscle is lengthened further its stiffness was not maintained as the slope of the work path decreases. After the antagonistic force was removed and the muscle overcame inertia the MTU began to shorten. Unlike the model, the force produced by the isolated muscle is significantly smaller during the shortening period than the lengthening period. As a result, a significant amount of energy is dissipated (clockwise encirclement of the work loop). Therefore, the CE in the isolated muscle was likely stretched significantly more than predicted by the model.

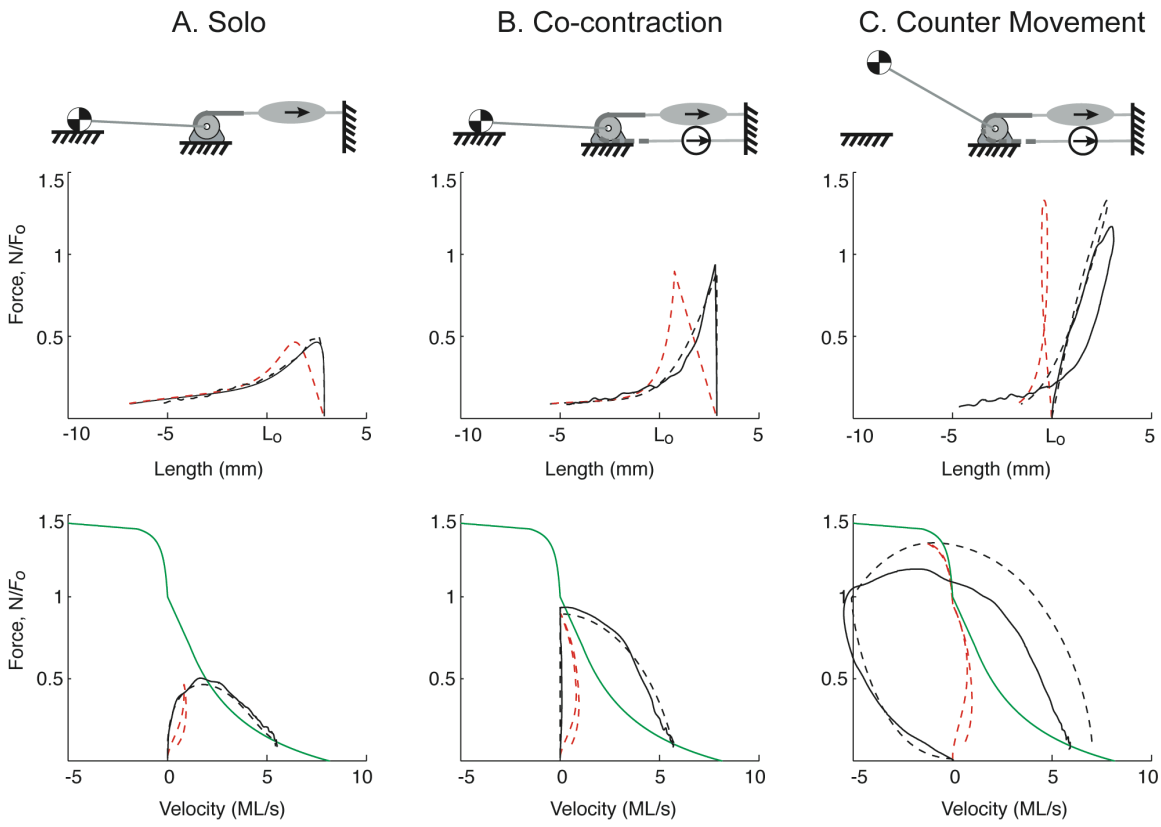


**Figure 3.6: Work loop and force–velocity relationships of the frog semimembranosus during a jumping task.** Each column describes the dynamic F–L and F–V relationship properties of the muscle for a different jump strategy: (A) Solo, (B) Co-contraction, (C) Countermovement. The model MT trajectories are shown with a dashed black line and the CE trajectories shown with a dashed red line. The mean experimental MT results are illustrated with a thick black line. The green line depicts the force–velocity relationship used in the muscle model.

For all the strategies the shape of the dynamic force-velocity curve, which is significantly different than that measured using isotonic contractions, explains the power amplification (Figure 3.6). When the MTU began to shorten, the force produced is greater than that predicted by isotonic contractions thus improving power production. However, the CE, which was defined by isotonic experiments, did not exceed the isotonic F–V

relationship. The dynamic F−V relationship was exaggerateby the co-contraction strategy (Figure 3.6 B). During co-contraction the muscle produced a force while the MTU length remained constant. The CE shortened during this time period approaching a steady-state length (velocity approaches 0). After the antagonistic force was removed, CE remained approximately isometric while the SEEs rapidly shortened. As a result, the muscle force is near its isometric level even though the MTU is shortening rapidly, thus amplifying the power produced.

## Discussion

We have shown that SEEs can temporally redistribute energy produced by the CE and amplify the power applied to the body during a jump. The energy stored in SEEs can be rapidly released and is not limited by cross-bridge dynamics resulting in substantially greater power transfer. Similar to *in vivo* power estimations, we measured, in an isolated muscle, peak powers that were considerably greater than the maximum isotonic power. Even during the solo strategy, which did not use any antagonistic forces, the SM produced peak powers significantly greater than its maximum isotonic power. Due to gravity and inertia, some energy was stored in the in SEEs before the MTU began to shorten. Some of the stored energy was later released when the muscle shortened amplifying power production.

The kinematics produced by the solo and co-contraction jump strategies are similar to that measured *in vivo* (Table 3.2). Our experimental results show that the MTU shortened approximately 25% and 23% during the solo and co-contraction strategies respectively. Previously published *in vivo* studies measure approximately the same

change in MT length in *Rana pipiens* (Lutz and Rome, 1996a) and *Bufo marinus* (Gillis and Biewener, 2000). Additionally, the duration of shortening in the solo strategy (84 ms) is similar to the shortest durations measured *in vivo* (~ 80 ms) (Lutz and Rome, 1996a). Further, the duration of shortening in our co-contraction strategy (153 ms) is comparable to the longer durations measured *in vivo* (141 ms) (Peters et al., 1996).

During the solo and co-contraction strategies, when the muscle only shortened, the Hill-type model accurately predicted the function of the isolated muscle. During the countermovement strategy, however, the peak power produced by the isolated muscle was significantly smaller than the model prediction. During the first 25 ms of the movement the MTU stretches approximately 0.8 mm and the model results match the experimental data well. Stretching the MTU further resulted in a reduction in muscle stiffness that was not predicted by the model (Figure 3.6 C). As a result, the MTU stretched significantly more than expected and produced less force. The peak power, however, was still significantly greater than that produced using the other strategies. Nonlinearities which are not included in our Hill-type model (Sandercock and Heckman, 1997) may explain the differences measured between the model prediction and the

**Table 3.2: Comparison with *in vivo* measurements of frogs jumping.**

| Source | Species | Length Shortened (% ML) | Shortening Duration (ms) | EMG Duration (ms) |
|---|---|---|---|---|
| Peters/Kamel 1996 | *Rana Pipiens* | 9 | 141 | 84.8 |
| Lutz and Rome 1996 | *Rana Pipiens* | 25.4 | 80 | 65 |
| Gillis 2000 | *Bufo marinus* | ~25 | 127 | 91 |
| **Strategy** | | | | |
| Solo | | 25 | 84 | |
| Co-contraction | | 23 | 153 | |

isolated muscle data. Still, Hill-type muscle models can predict the function of isolated muscle during simple, but behaviorally relevant models.

Our model predicted that the muscle behaves like a spring in the countermovement jump. The CE remains approximately isometric while the SEEs stretched and shortened to absorb and release work (Figure 3.6 C). The average power produced by the agonist (SM) is close to zero as the countermovement action was very elastic. This muscle function is similar to that measured during locomotion in several other animals. During the stance phase of level running in turkeys, the fibers in the lateral gastrocnemius isometrically produce force to support body weight while the aponeurosis, the major source of compliance, absorbs and releases kinetic energy from step to step (Gabaldon et al., 2004; Roberts and Scales, 2002). This passive recovery of mechanical work accounted for more than 60% of the total work produced by the MTU. Similarly, in the plantaris and lateral gasctrocnemius of the hopping tammar wallaby, elastic recovery of work stored in the tendon accounts for more than 90% of the work produced by the MTU (Biewener et al., 1998).

Our measurements indicated that the frog SM, which does not have a long tendon, is capable of storing significant amount of energy. Although the Hill muscle model lumps series elasticity into a single element, there are several sources of series elasticity in skeletal muscles including the thick (Huxley et al., 1994) and thin (Higuchi et al., 1995) filaments, the crossbridges (Ford et al., 1977), as well as tendinous structures. The aponeurosis in the frog semitendinosis has shown to be the main source of series compliance (Kawakami and Lieber, 2000; Lieber et al., 1991). Fixed-end contractions in

the semitendenosus (Kawakami and Lieber, 2000) and SM (Ahn et al., 2003) reveal that the sarcomeres can shorten approximately 10% even though the MT length is held constant while the muscle is maximally activated. This compliance is larger than that we measured (7.1%). Further, other non-muscular sources, like bones, can be sources of series compliance and help increase the energy that the frog can store prior to forward movement.

Closed-loop isolated muscle protocols (Farahat and Herr, 2005; Lin and Rymer, 2000) have tremendous potential for improving our understanding of motor control principles. These novel techniques allow us to re-create the complicated interactions that occur between skeletal muscles and the environment during movements. Using real-time feedback we examined the mechanical properties of muscle as it worked against a dynamic load that included an inertial and gravitational component as well as prescribed antagonistic forces. Our results could not have been acquired using traditional muscle physiology techniques.

# CHAPTER 4

# INTRINSIC MUSCLE CONTRIBUTIONS TO DYNAMIC STABILITY DURING A BOUNCING GAIT

## Introduction

Engineered systems are unable to match the animal neuromuscular system's ability to maintain dynamic stability during locomotion over complex terrains. The ability to withstand unexpected perturbations arises from the integration of sensory mechanisms and the intrinsic mechanical properties of muscle. But, perturbation responses based on sensory feedback are subject to time delays limiting their contribution during rapid movements. Muscles, however, can respond instantaneously to perturbations, altering the force they produce without any change in their neural activation pattern (Loeb et al., 1999). In this study, we evaluate the ability of muscle, without the aid of sensory feedback, to stabilize locomotion.

During rapid locomotion, animals often exploit an efficient bouncing gait that exchanges kinetic and gravitational energy with elastic potential energy during each step (Cavagna et al., 1964). During the first half of stance phase, kinetic and gravitational energy is stored as elastic energy in the limb. During the second half, this elastic energy is recovered to accelerate the body. In analyzing locomotion, many researchers adopt a spring-mass model, where a point mass represents the body and the massless spring represents the compliance of the limbs, that theoretically explains the energy exchange of a bouncing gait (Blickhan, 1989; McMahon and Cheng, 1990). Although spring-mass

systems can maintain stable periodic gaits (Seyfarth et al., 2002; Seyfarth et al., 2003), they are unable to maintain the total system energy (see Discussion)

To facilitate the bouncing gait, muscles can function to store and release energy like springs (Alexander and Bennet-Clark, 1977; Roberts, 2002). Skeletal muscles are comprised of two primary types of mechanical elements: the contractile element (CE), which is comprised of the cross-bridge filaments, and series elastic elements (SEEs), which include the tendon, aponeurosis, and intramuscular elements (Roberts, 2002). Muscle forces, which are generated by the CE, are transferred to the skeletal structure via SEEs. These spring-like elements stretch proportionally with muscle force and are capable of storing energy. During a bouncing gait, the CE remains approximately isometric while SEEs initially stretch to store energy and then shorten to release energy (Alexander and Bennet-Clark, 1977; Dickinson et al., 2000). As a result, muscles function to recycle a substantial amount of energy from step to step (Biewener et al., 1998; Roberts et al., 1997).

To stabilize perturbations during a bouncing gait muscles must also produce and dissipate energy. The ability of the muscle to produce and dissipate energy is facilitated by the inversely proportional relationship between force produced by the CE and its velocity (Hill, 1938). When stretched, the CE dissipates energy and when shortened, the CE produces energy. Perturbations that add energy to the body and increase the landing velocity during a bouncing gait may stretch the CE, which would dissipate energy and begin to return the body to its original steady-state trajectory. Perturbations that remove energy from the body and decrease the landing velocity would allow the CE to shorten

and restore the lost energy.

We hypothesize that the intrinsic properties of muscle, without sensory feedback, can stabilize a bouncing gait. To evaluate the stabilizing properties of muscle, we extend the spring-mass system by replacing the spring with a muscle to more accurately replicate the mechanics of a bouncing gait. We investigate the energetics of the bouncing gait and assess the muscle's ability to recycle, produce, and dissipate energy. Using novel experimental techniques we test our hypothesis experimentally. To identify the function of the CE and SEEs, which are distributed throughout the muscle, we also use a computational muscle model with discrete contractile and elastic elements.

## Methods

We evaluated the ability of intrinsic muscle properties to stabilize a bouncing gait using mathematical and *in vitro* muscle models of the frog (*Rana pipiens*) semimembranosus (SM). Extending previous studies (Wagner and Blickhan, 1999), that were limited by mathematical models, we examined isolated muscles during the ground contact phase of a bouncing gait. In addition, we developed a three-element muscle model to determine the function on the CE and SEEs. By combining computational and experimental methods we exhaustively tested our hypothesis and leveraged the benefits of both techniques. This section provides details of the models used, experiments conducted, and analysis techniques applied.

### Bouncing Gait Mechanics

In a manner similar to the one-dimensional spring-mass model, we examined the function

of one muscle working against an inertial load under a gravitational field (Figure 4.1). Only the stance phase, when the muscle can exert forces on the mass, is considered.

$$GF_m - F_g = M\ddot{x}_d \qquad (4.1)$$

The force the muscle produces ($F_m$) acts on an inertial load ($M$) and gravitational ($F_g$)

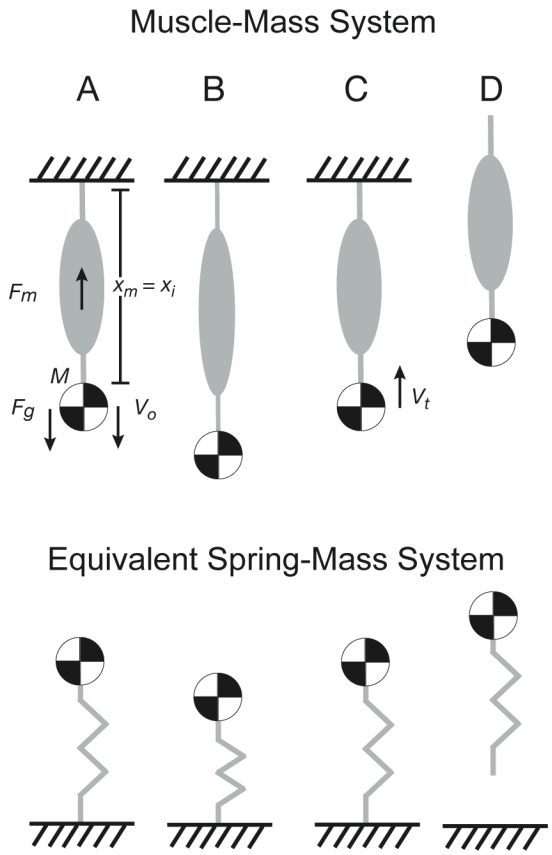


**Figure 4.1: Mechanical context for a single muscle during a bouncing gait.** (A) An initial stretching velocity was applied to the load to simulate landing. The muscle stretched while absorbing and dissipating energy. (B) The muscle reached a maximum length and began to shorten. (C) The muscle shortened and accelerated the load. The load leaves the ground with a takeoff velocity when the muscle returned to its original length. (D) The flight phase of the bouncing gait was not included in the model. We assumed that velocity at which the mass left the ground was equivalent in magnitude to the landing velocity of the next step. The equivalent spring-mass system is shown at the respective phase of the gait.

load. The gravitational force and mass were chosen to approximate the load the frog SM works against *in vivo* (see previous chapter). The muscle force gain term ($G$) is a constant scalar used to normalize the forces in the isolated muscle such that it matched the force in the model. The desired muscle-tendon (MT) length ($x_d$) is determined by (Equation 4.1). For all conditions, the initial muscle length ($x_o$) was set to $L_o$.

For the *in vitro* experiments, a closed-loop controller functioned to minimize the difference between the actual ($x_m$) and desired ($x_d$) MT lengths. The linear actuator that stretched and shortened the muscle has an associated inertia and therefore cannot perfectly track the desired MT length ($x_d$). To better match *the in vitro* experiments, the dynamics of the muscle length controller and actuator were considered when using the computational muscle model:

$$x_m = H(x_d - x_m)$$

where $H$ is a transfer function that includes the controller transfer function, motor inertia, motor constant, and current saturations.

**Computational Muscle Model and Closed-Loop Experiments**

To separate the function of the contractile and series elastic elements we conducted parallel isolated muscle experiments and simulations. The isolated muscle experiments provided real data and were used to determine the accuracy of the computational muscle model. The muscle model provided access to the kinematics of the CE and SEEs, allowing us examine their function.

Muscle Model

We developed a Hill-style mathematical muscle model (Zajac, 1989) of the frog semimembranosus (SM). Using the muscle model we estimated the energetics and kinematics of the SM during the ground contact phase of a bouncing gait. The details of the muscle model can be found in Chapter 3.

Closed-Loop Experiments

In order to validate our computational model and energetic predictions, we examined the overall performance of living muscles during a bouncing gait. Using closed-loop techniques we coupled the isolated frog SM to the load described in the previous section. This technique is similar to that used in previously published studies (Farahat and Herr, 2005; Lin and Rymer, 1998) and in Chapter 2. The virtual connection between the muscle and computational load was accomplished using the following closed-loop approach:

1) Electrical stimulation activates the muscle producing a force.
2) The force produced by the muscle is measured and used to accelerate the load. Gravity and antagonistic forces can also act on the load.
3) The resulting position of the load is computed and specifies the desired length of the muscle-tendon unit (MTU), thus closing the loop.

All surgeries were performed according to procedures approved by the Institutional Animal Care and Use Committee at the Georgia Institute of Technology (Protocol

#A07033). Prior to the surgery, frogs (*Rana pipiens*) were anestheized with tricaine methanesulfonate (MS-222, 1 g $L^{-1}$). The frogs were then double pithed. The SM, still innervated by its nerve and attached to bone chips, was removed along with a portion of the sciatic nerve. Small metal clamps were used to attach the proximal bone chip to a load cell and the distal bone chip to a linear actuator. The load cell measured the force the muscle produced and the linear actuator controlled and measured its length. The entire muscle was submerged in a bath (~21 °C) of oxygenated (95% oxygen, 5% carbon dioxide) Ringer's solution (pH 7.1). A suction electrode was used to activate the muscle via the sciatic nerve. For all conditions the muscle was maximally activated (1 mA, 60 Hz, 100 μs).

At the beginning of every experiment the length ($L_o$) at which the muscle can produce a maximal isometric force was experimentally determined. The force gain term ($G$) was set in (Eq, 1) such that the isometric force matched that of the model. No other normalizations were applied. Between every other trial the isometric force was measured and the gain term ($G$) was increased to account for fatigue. Once the isometric force dropped 15% data collection was stopped.

**Experiment Protocol**

To simulate different landing velocities and examine the stance phase of a bouncing gait, the initial velocity ($\dot{x}_o$) was varied in both, the isolated and computational muscle. The system was considered to be in stance phase as long as the MT length ($x_m$) is greater than the initial length ($L_o$). The initial length was considered to be "full extension" and lengthening the MTU flexed the 'body'. After the MTU returned to its initial length ($L_o$),

data collection was stopped as the system was considered to be off the ground. The magnitude of the takeoff velocity in one step was equal to the magnitude of the landing velocity in next step. A periodic gait was achieved when the landing and takeoff velocities are equal in magnitude.

The isolated and computational muscles were activated 10 ms before the initial landing velocity was applied. The muscle takes approximately 10 ms to reached an active state and start producing force. During the aerial phase of a bouncing gait the extensor muscles are likely activated before making contact with the ground. In a multi-segment model, extensor muscles can work against the load provided by different limb segments and produce a force. In our simplified model, the muscle is unable to do so and pre-activation by 10 ms insures that activation kinetics do not play a major role during the ground contact phase.

**Dynamic Stability Analysis**

The kinematics of a bouncing gait can be explained by three output metrics: ground contact duration, takeoff velocity or jump height, and frequency. Knowledge about any two of these states is sufficient to determine the third. In our system, however, because the muscle properties are constant, examining just the takeoff velocity is sufficient.

Dynamic stability can be analyzed using a return map. A return map plots a specific variable at specific point in space from one step ($y_i$) to the next step ($y_{i+1}$). We examined the landing velocity at the MT length ($L_o$). A fixed point, therefore, occurs when the variable of interest is constant from step to step ($y_{i+1} = y_i$). Further, the fixed point is

stable if the return map passes the fixed point with a slope whose magnitude is less than 1 (Seyfarth et al., 2002). Of course, the magnitude of the landing velocity at step $y_{i+1}$ is equal to take magnitude of the takeoff velocity at step $y_i$.

## Results

In the context of the one-dimensional bouncing gait described previously, we measured the kinematics and energetics of the frog SM. We used both, experimental and computational methods, to determine how the CE and SEEs function together to form a stable gait. By examining the work produced by the muscle and performing a return-map analysis for different landing velocities, we showed that the intrinsic properties of muscle, without any sensory feedback, form a dynamically stable bouncing gait.

### Kinematics

We compared kinematics produced by the isolated and computational muscle and determined the function the CE and SEEs during the bouncing gait. In particular, we examined the muscle when it functioned to accelerate, maintain in steady state, and decelerate the bouncing gait.

Accelerating

For a small landing velocities the muscle-mass system left the ground at a greater velocity magnitude, indicating the bouncing gait is accelerated (Figure 4.2 A). During the first half of the stance phase, muscle force increased due to activation (activations starts at t = 0 s) but the MTU lengthened (solid and dashed black traces) due to the initial velocity (applied at 10 ms). The force produced by the muscle initially decelerated the

mass and then accelerated it (in the opposite direction) for the following flight phase. During the second half of stance phase, the MTU shortened and the muscle force declined. At takeoff, the model and isolated muscle were both still accelerating suggesting that the takeoff velocity would be even greater if the muscles had more room to extend (we define takeoff as the time when the muscle length has returned to its original length, $L_o$) (Figure 4.2 A, third row).

Although the MTU is initially lengthened, the model predicted that the CE shortened during the entire stance phase (dashed red trace). This suggests that the negative power produced by the MTU was not dissipated but was stored in SEEs (Figure 4.2 A, last row). However, because muscle force was near maximal at takeoff, only a small amount of energy was released by the SEEs to power the next flight phase. The release of energy from SEEs is evident when MT power is greater than CE power.

Due to the dynamics of the muscle length actuator, the initial velocity (applied at 10 ms) was not instantaneous for both the model and the isolated muscle. Further, the peak negative velocity has a greater magnitude than the prescribed landing velocity. As described previously, during the experiments the response of the muscle length actuator was limited and could not achieve infinite accelerations. The dynamics of the actuator were also considered in the muscle model so that both methods could be compared.

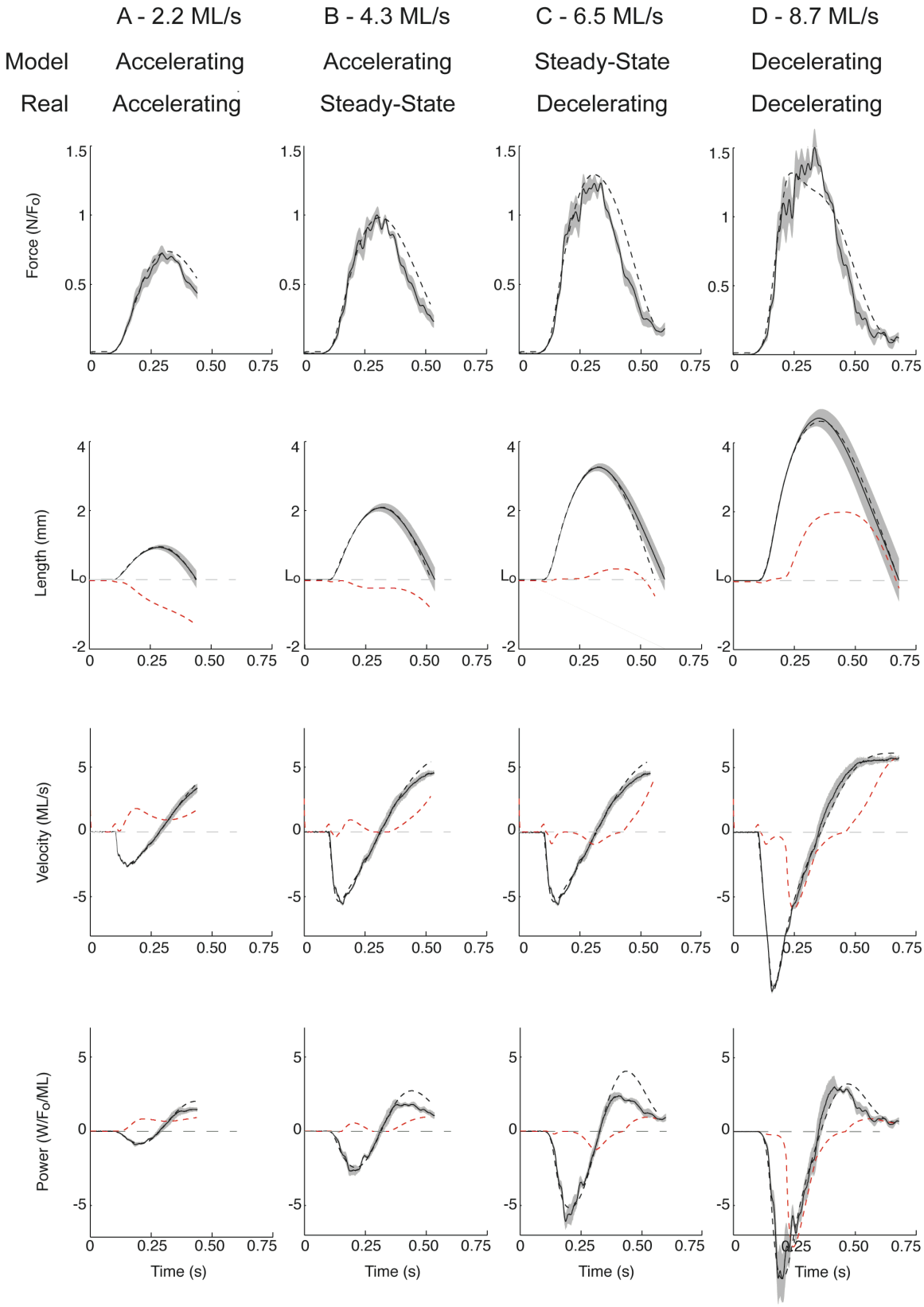
A - 2.2 ML/s
B - 4.3 ML/s
C - 6.5 ML/s
D - 8.7 ML/s
Model
Accelerating
Accelerating
Steady-State
Decelerating
Real
Accelerating
Steady-State
Decelerating
Decelerating
Force (N/Fo)
Length (mm)
Lo
Velocity (ML/s)
Power (W/Fo/ML)
Time (s)

**Figure 4.2: Model and experimentally measured muscle forces, kinematics, and energetics.** Each column shows the muscle force, length, velocity and power for different landing velocities. Each landing velocity provides an example of the bouncing gait during an accelerating, steady-state, and decelerating stance phase for the isolated and model muscle. In all panels, the trajectories end when the muscle length has returned to its original length and the mass is assumed to have left the ground. The model MTU trajectories are shown with a dashed black line and the CE trajectories shown with a dashed red line. The mean experimental MTU results are illustrated with a thick black line. The shaded regions indicate one standard deviation above and below the mean. The data for each column was measured from seven frogs, except for column D, which was measured from six frogs. Rows 1 and 2 show the muscle force and length time responses respectively. The CE and MTU always produce the same force. The length of the SEEs, which is proportional to muscle force, is the difference between the MT (black) and CE (red) length. Row 3 shows the velocity of the MTU and CE. Shortening velocities are positive and lengthening velocities negative. The last row plots the instantaneous power produced by the muscle.

Steady-State

The steady-state landing (or takeoff) velocity differed greatly for the isolated and model muscle. Similar to the accelerating condition, the force produced by the muscle first acted to overcome the landing velocity and then accelerated the muscle for the next flight phase. The model kinematics matched that of the isolated muscle during the first half of stance phase when the muscle lengthened. However, when the MTU was shortening, the model over predicted the force produced by the isolated muscle (Figure 4.2 B). As a result, the model muscle over predicted the takeoff velocity of the isolated muscle.

During the model steady-state hopping gait, the CE remained approximately isometric during the entire stance phase (Figure 4.2 C, second row). The CE initially lengthened slightly and then shortened (evident in the velocity trajectory, third row), and therefore dissipated and produced energy (last row). Of course, to maintain the steady-state gait, the energy produced and dissipated by the CE must be equal. At this landing velocity,

the isolated muscle decelerated the gait. Again, the model matches the force and kinematics produced by the isolated muscle while it lengthened. However, the predicted force and power production during muscle shortening was greater than that measured in the isolated muscle.

Decelerating

For large landing velocities, the muscle-mass system left the ground at slower velocity magnitudes, indicating that the bouncing gait decelerated (Figure 4.2 D). In response to the initial velocity, the muscle force reached values greater than its maximum isometric force (first row). However, the muscle force was not sufficient to accelerate the load to a takeoff velocity that matched the landing velocity (in magnitude). Once more, the computational model over predicted, to smaller degree, the forces experimentally measured when the muscle was shortening. At takeoff, the MT velocity had reached a maximum and the acceleration was almost zero (third row). As a result, further extension of the body, or shortening of the muscle, would not have increased the takeoff velocity.

Unlike the previous conditions, the initial landing velocity significantly lengthened the CE, facilitating energy to be dissipated. Although the CE approximately returned to its initial length at takeoff (second row), it dissipated more energy than it produced (last row).

**Energetics and the Return Map**

In order to accelerate and decelerate the bouncing gait, the muscle must produce and dissipate energy respectively. We examined the total work produced by the isolated and

model muscle for different landing velocities (Figure 4.3). For slower landing velocities, the muscle produced work facilitating the acceleration of the bouncing gait. For quicker landing velocities, the muscle dissipated work enabling the system to decelerate. At the landing velocity where the muscle produced zero work a steady-state bouncing gait existed. Here, the muscle produced as much work as it dissipated and the system left the ground at a velocity that is equal in magnitude to the landing velocity. The stead-state landing velocity for the model muscle is greater than that measured in the isolated muscle.

To assess the function the muscle during stance phase and determine how energy is produced, dissipated, and stored, we also examined the work loops and dynamic force–velocity relationships (Figure 4.4). The work loop plots muscle force as a function of

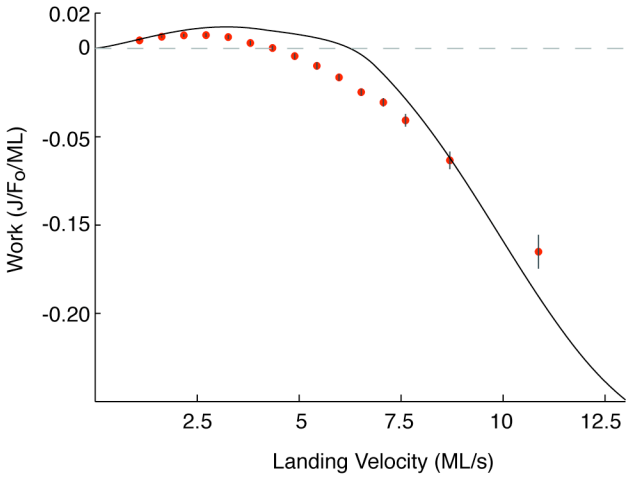


**Figure 4.3: The work produced or dissipated by the muscle for different landing velocities.** The black line indicates the mathematical model prediction and the dots represent the data collected from isolated muscles. For most landing velocities, the model muscle produced more work than measured by the isolated muscle. An average of five experiment trials (each from a different frog) were conducted for each landing velocity. The vertical grey bars indicate one standard deviation above and below the mean.

muscle length (first row) and allowed us to visually examine muscle energetics (Josephson, 1985). In all conditions, SEEs facilitated the MTU to act beyond the force–velocity constraint (see Chapter 3).

Accelerating - During the accelerating conditions (Figure 4.4 A), the CE shortened and produced energy, automatically accelerating the gait. Although the initial velocity initially lengthened the MTU, the CE shortened and produced energy during entire stance phase. The counter clockwise encirclement of the work loop indicates the muscle has produced energy. To complete the work loop, imagine a vertical line connecting the final force with the initial force (the lengths are the same) on the MT trajectory. At the end of the stance phase, the MT length is significantly longer than CE length, indicating that the SEEs were stretched and energy stored in them was wasted.

Steady State - During the steady-state trajectories (Figure 4.4 B, C), the muscle dissipated and produced energy and therefore did not act like a perfect spring. Although the length of CE did not change significantly, its velocity did. Initially, the CE lengthened and dissipated energy (Figure 4.4 C). The CE velocity approached but did not enter the plateau region of the lengthening force–velocity relationship. Eventually, the CE shortened and produced energy, offsetting the energy dissipated earlier. The energy dissipation and production can be visualized in the work loop and the clockwise and counter clockwise encirclements respectively.

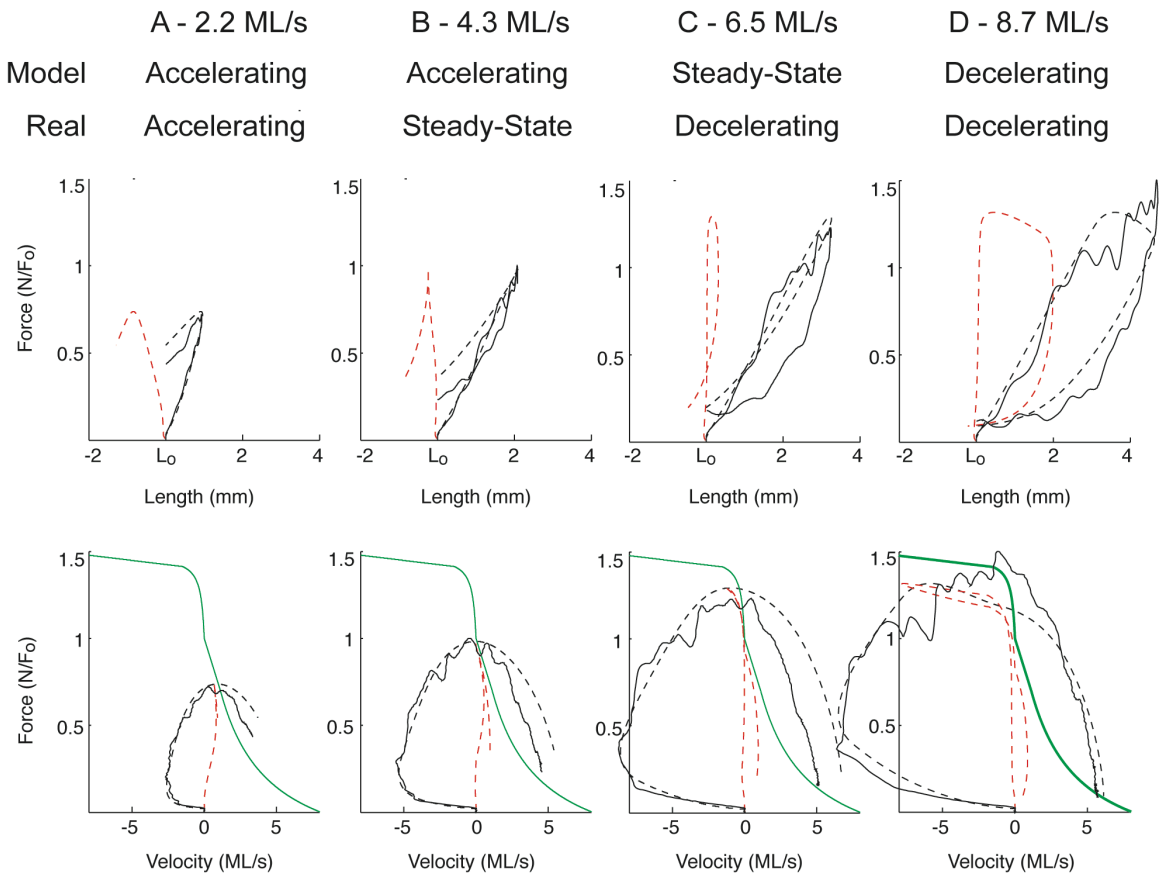


**Figure 4.4: Model and experimentally measured work loops and force–velocity relationships.** Each landing velocity (column) provides an example of the bouncing gait during an accelerating, steady-state, and decelerating stance phase for the isolated and model muscle. The first row plots the work loop and visually shows the energy produced (counter-clockwise encirclements) and dissipated (clockwise encirclements). The second row compares the force–velocity relationship of the muscle during bouncing gait with a typical isotonic force–velocity curve (green). In all panels, the trajectories end when the muscle length has returned to its original length and the mass is assumed to have left the ground. The model MTU trajectories are shown with a dashed black line and the CE trajectories shown with a dashed red line. The mean experimental MTU results are illustrated with a thick black line. The shaded regions indicate one standard deviation above and below the mean. The data for each column was measured from seven frogs, except for column D, which was measured from six.

Decelerating - During decelerating stance phases, the plateau region of the lengthening force–velocity relationship facilitates the dissipation of energy (Figure 4.4 D). In response to the initial (landing) velocity, the CE stretched at large velocities and entered the plateau region of the of the force–velocity. In this region, the muscle reached its force-producing limit; stretching the CE faster would not have increase muscle force. Therefore, the SEEs had also reached their limit for energy storage. As a result, the muscle effectively dissipated energy and decelerated the gait. The energy dissipation is shown by the large clockwise encirclement of the work loop.

We performed a return map analysis on the takeoff velocity to assess the stability of the bouncing gait (Figure 4.5). Assuming a ballistic motion when the system is 'in the air', a periodic gait occurs when the takeoff velocity (or the landing velocity of the next step) is equal to the landing velocity (diagonal line). In the return-map this velocity is referred to as a fixed-point and corresponds to the velocity where the muscle has produced no work. The location and the behavior at the fixed point were different for the model and isolated muscle. The model and isolated muscle both have a slope with magnitude less than 1 as they pass the fixed-point, indicating that the gait is stable. The behavior of the computational and isolated muscle, however, was different at the fixed point. The isolated muscle had a positive slope, whereas the model has a negative slope. The negative slope indicates that a perturbed system will overshoot its return to the steady-state trajectory. For example, if the system is perturbed such that it lands at a velocity slightly greater than its fixed-point velocity, it will first decelerate below the fixed-point velocity and then accelerate back towards the fixed-point. The closer the slope is to -1, the more over/undershoot oscillations will occur before the system settles to its steady-

state trajectory. This behavior is analogous to an underdamped system. A positive slope indicates that the system returns to the steady-state trajectory without overshoot, analogous to an overdamped system.

**Recovery**

For different landing velocities, we calculated the amount of energy stored and released by the SEE in our computational model (Figure 4.6 A). Generally, as the landing velocity increased, the SEE recovered more energy. For landing velocities greater than 8.5 ML/s, the amount of energy recovered initially decreased before increasing again. The initial decrease occurred when the CE velocity entered the plateau region of the force–velocity relationship. In the plateau region, muscle force remained constant and

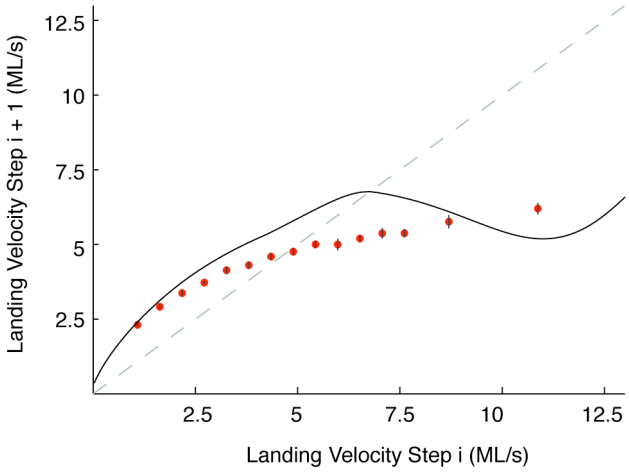


**Figure 4.5: The return map analysis for the model and isolated muscle.** The return map examines the relationship between the takeoff and landing velocity. Because the takeoff velocity for the current step is the landing velocity for the next step, a fixed point occurs when the takeoff velocity is equal to the landing velocity (in magnitude). The model muscle (solid line) over predicts the fixed-point takeoff velocity measured in the isolated muscle (dots). The model and isolated muscle have stable fixed points as their return maps cross the diagonal with a slope of magnitude less than 1. An average of five experiment trials (each from a different frog) were conducted for each landing velocity.

thus no more energy could be stored in the SEEs. In addition, less energy was recovered from the SEE because the CE did not achieve a fast shortening velocity and the muscle force at takeoff was large. The energy recycled by the SEE increased again for even greater landing velocities where the CE was stretched to such great lengths that the parallel elastic element helped increase muscle force. The increased muscle force resulted in an increase in the storage of energy in the SEEs and improved the total energy recovered by the SEEs. The energetic recovery due of the elasticity in the parallel elastic element, the passive force–length property, was not considered.

We also examined the elastic recovery of the muscle by measuring the fraction of energy recycled by the SEEs normalized to the kinetic energy of the system at the beginning of the stance phase (Figure 4.6 B). At the fixed point (vertical bar), our model predicts that the muscle recovers over 75% of the system's initial kinetic energy and therefore only had to produce a small amount of energy to maintain the steady-state gait. For velocities beyond the fixed point, the muscle dissipated a substantial amount of energy and therefore a smaller percentage of energy was recovered. In addition, we noticed in the isolated muscle that the peak muscle force and the muscle force at takeoff were approximately equal to that predicted by the model. Because SEEs stretch and shorten proportionally with muscle force, a significant amount of energy was likely also recovered in the isolated muscle.

## Discussion

The initial response to a perturbation is influenced entirely by the intrinsic properties of muscle. In this study, we examined how the contractile and elastic elements in muscle function to maintain dynamic stability, without the aid of sensory feedback, during a bouncing gait. Our results show that muscles can automatically manage mechanical energy to maintain a stable bouncing gait. In addition, our simulations suggest that SEEs in muscle help produce an efficient gait by recycling a significant amount of energy from one step to the next.

Our results reveal that the mechanical properties of muscle can react to different loading conditions and alter the muscle's function without a change in its activation pattern. The use of such 'intelligent' mechanics may reduce the effort (Blickhan et al., 2007) and

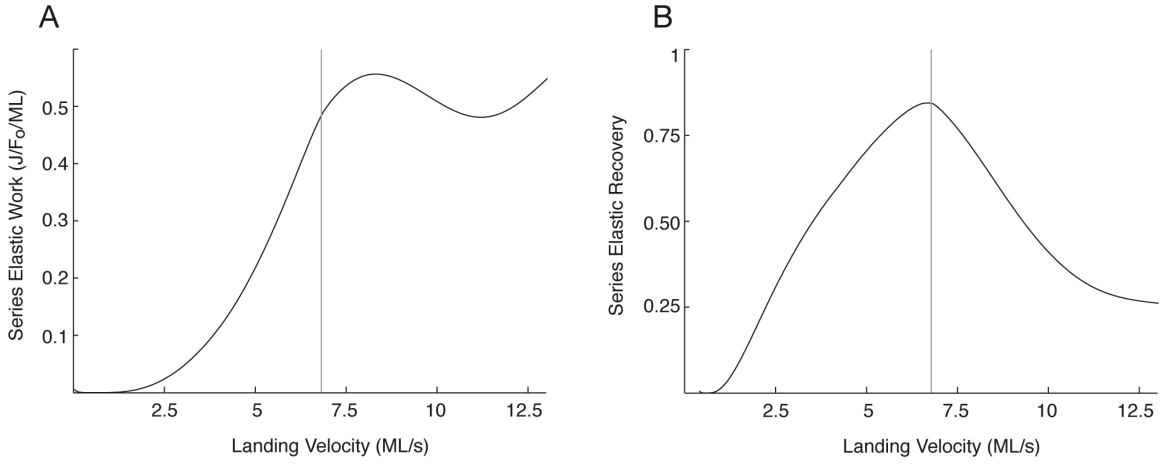


**Figure 4.6: Predicted elastic recovery by the series elastic element during the bouncing gait.** Panel A shows the energy applied to the load by the SEE which stored some of the systems kinetic energy at the beginning of the stance phase. Panel B shows the elastic recovery, the energy recycled by the SEE normalized to systems initial kinetic energy. The vertical grey line marks the steady-state landing velocity. During the steady-state gait, approximately 80% of the kinetic energy is recycled every step.

architecture of neural control mechanisms. Our results suggest that animals may not have to employ active control to decrease or increase the speed of their gait, instead they may be able to simply set a new muscle activation level and mechanical properties of muscle would naturally entrain to the new speed. Similar control simplifications are evident during locomotion in other species. The guinea fowl, for example, does not significantly change the activation (EMG) duration, intensity or phase of its lateral gastrocnemius when walking on an incline compared to level ground (Daley and Biewener, 2003). The muscle's average force, net strain and work production, however, are automatically modified to manage load requirement of incline locomotion. Humans instantaneously change the stiffness of their legs when running across different viscoelastic substrates such that the combination of leg and surface stiffness remains unchanged (Ferris et al., 1999; Ferris et al., 1998). Although the control of leg stiffness likely arises from several mechanisms, the immediate response suggests that intrinsic muscle properties play a substantial role. The intrinsic properties of muscle may facilitate robust control of locomotion without the need for precise neural control.

Our computational model predicts, during a steady-state gait, that the SEEs in the frog SM can recover over 75% of the kinetic energy from the previous aerial phase and apply it to accelerate the load for the next aerial phase. As a result, the CE only has to generate a small amount of energy every step to maintain locomotion. During accelerating stance phases, SEEs are less effective and recover less energy. However, our results indicate that if there was more kinematic room for the MTU to shorten, it could further accelerate the load and the SEEs would recover more energy. Therefore, during accelerating stance phases, landing in a slightly flexed position would give the extensors more room to

shorten and increase the takeoff velocity. During the stance phase of level running in turkeys, the fibers in the lateral gastrocnemius isometrically produce force to support body weight while the aponeurosis, the major source of compliance, absorbs and releases kinetic energy from step to step (Roberts et al., 1997). This passive recovery of mechanical work accounted for more than 60% of the total work produced by the MTU. Similarly, in the plantaris and lateral gasctrocnemius of the hopping tammar wallaby, elastic recovery of work stored in the tendon accounts for more than 90% of the work produced by the MTU (Biewener et al., 1998).

SEEs in muscle function to store and release energy and help improve the efficiency of locomotion (Cavagna et al., 1977; Cavagna and Kaneko, 1977; Cavagna et al., 1964) (Alexander and Bennet-Clark, 1977). Our energetic recovery estimates do not translate to efficiency because there is a metabolic cost associated with activating muscles even if they do not produce any force. Our computational model, however, suggests that the CE is approximately isometric during the stance phase of a bouncing gait. Therefore, fewer muscle fibers have to be recruited to produce the same force, as compared to conditions when the CE is shortening. This economic force generation likely results in less chemical energy consumption by the muscle (Biewener et al., 1998). A lengthening CE produces even more force, suggesting that the efficiency is even greater. During conditions when the CE lengthens significantly, the system is dissipating energy and decreasing the speed of the gait.

The self-stabilizing properties of muscle may work synergistically with neural control strategies. In two-dimensional spring-mass bouncing gaits, recent studies have shown

that a feedforward strategy that automatically changes the angle of attack can stabilize the maximum height of the gait (Geyer et al., 2005; Seyfarth et al., 2002; Seyfarth et al., 2003). Since springs are unable to produce or dissipate energy, changing the angle of attack only serves to redistribute the system energy in the vertical and horizontal directions. Therefore, even though the maximum height of the gait can be maintained, other parameters, such as step length, have to change. However, combining this feedforward strategy with the mechanical properties of muscle may improve stability and facilitate a quicker return to the steady-state trajectory after a perturbation.

Small errors in the predicted kinematics of the CE may explain the difference in function between the model and isolated muscle. During the muscle-shortening phase of the gait, the model over predicted the force produced by the isolated muscle. If the CE in the isolated muscle shortened at a slightly faster velocity or was at a shorter length compared to the model prediction, force produced by the isolated muscle would be smaller than that predicted. Nonlinear properties, which are not considered in the three-element, such as shortening deactivation (Edman et al., 1993; Josephson and Stokes, 1999), likely do not explain the differences between the isolated and model muscle. The effect of shortening deactivation is proportional to CE shortening distance and inversely proportional to CE velocity. Our results, however, suggest that the difference in force, between the model and isolated muscle, is greatest when the CE shortening is minimal and shortening velocity is maximal.

This work is an important step towards advancing our understanding of muscle mechanics, leading towards improved actuators with realistic mechanics that have the

potential to progress robotic and other engineered systems. Mimicking the mechanical properties of muscle in robot actuators may yield improved maneuverability, stability, and speed during locomotion (Blickhan et al., 2007; Herr et al., 2001; Pratt, 2000; Pratt, 2002). Although the elastic properties of muscle have inspired a variety of new robot actuators (Migliore et al., 2007; Pratt, 2002), the velocity dependent properties of muscle are rarely considered. Using actuators that imitate the force–velocity relationship of muscle may help maintain steady-state system energetics and further improve stability.

# CHAPTER 5

# CONCLUSIONS

Animals have evolved robust neuromuscular strategies that underlie their impressive agility and speed during locomotion over a variety of natural environments. Muscles, the most peripheral layer of the neuromuscular system, produce forces that give rise to movement and interact with the environment with unique mechanical characteristics. Understanding the principles of animal movement and taking inspiration from the function of muscles will serve as a foundation to advance engineered systems. In this dissertation, we applied experimental and computational techniques to understand how the mechanical elements in muscle can facilitate two important tasks during locomotion: power production and dynamic stability. To investigate the mechanical properties of muscle, we initially developed a closed-loop system that virtually couples an isolated muscle with a computational or physical mechanical load. We used this system to demonstrate the effects and importance of intrinsic muscle properties during movements.

Throughout this dissertation we showed that, given the same neural activation pattern and no sensory feedback, a muscle is still able to advantageously function in a variety of different manners: producing, dissipating, and absorbing energy. Movement is the result of coordinated feedback and feedforward interactions between the central nervous system, the musculoskeletal system, and the physical environment. Although sensory feedback is an important mechanism that affects movement, this research is focused on only the mechanical interactions between muscles and the external environment. In

particular, we examined how intrinsic muscle properties can function to manage muscle energetics during movements. In all our studies, we maximally activated a muscle while providing different mechanical frameworks. Due to only the different loading conditions, the resulting muscle energetics were substantially different as the muscle acted as motor, brake, or spring. Therefore, we demonstrate that the function of muscle cannot be discerned from examining exclusively its electrical activation, but also requires an understanding of the mechanical context in which the neural control is applied. Neural control strategies acting in concert with musculoskeletal strategies facilitate the wide range of movements produced by animals. In this chapter, we provide a summary of our results, and draw implications about the mechanical properties of muscle and their effect on neural control.

## Technical Innovation

Although, classical open-loop experimental control is highly effective for isolating mechanical components of the three-element muscle model, it has limited ability to probe emergent properties of the complete model during dynamic movements. The three-element muscle model is deeply ingrained in our understanding of muscle mechanics and has defined the context in which muscle mechanics are measured. Traditional open-loop muscle physiology experiments were cleverly designed to isolate and evaluate particular mechanical properties of that model. For example, under isotonic loads (Hill, 1938), the muscle produces a constant force and shortens at a constant velocity, thus isolating the force–velocity relationship of the just the contractile element. The validity of the model and of these fundamental properties derives from their ability to predict muscle function during a variety of dynamic movements. Mathematical muscle models reveal complex

emergent behaviors that arise from the integrative action of simple mechanical properties. Mathematical predictions, however, have not been validated using living muscle tissue because of the limited open-loop nature of classical experimental methods.

Closed-loop systems (Farahat and Herr, 2005; Lin and Rymer, 1998) enable investigation of muscle as it works against complex loads, and thereby reveal interactions between the components of the three-element model. Under open loop control, an isolated muscle behaves as a first-order system, driven by elasticity and viscosity, very different from actual biological function. *In vivo*, muscle acts primarily against inertial loads as a second-order system, and it is only through the interaction between muscle and an inertial load that those second-order effects become manifest.

We applied closed-loop methods to facilitate a better understanding of muscle performance during dynamic movements that more accurately represent natural conditions. Specifically, we built a system that allows an isolated frog muscle to be connected to a variety of complex loads. Extending previously developed closed-loop systems, which are limited to computational loads, our system also facilitates the virtual embedding of the muscle directly into physical loads, allowing the muscle mechanics to control the movement of a robotic system. As a result, loads that are too complex to computationally estimate but can be reproduced with a physical system can also be applied to an isolated muscle.

## Scientific Contributions

We applied our closed-loop approach to investigate the function of living muscle during

dynamic locomotion-like tasks; previously these tasks have been typically examined with computational muscle models without knowing their validity under such dynamic conditions. Specifically, we identified the function of the contractile element (CE) and series elastic elements (SEEs) during power production in a jumping task, and determined their ability to produce a dynamically stable bouncing gait. To separate the functions of the CE and SEEs, we combined our experimental methods for isolated muscle with a mathematical three-element model. The integration of experimental data and model predictions provided insight into the integrative function of the musculoskeletal system.

The mechanical properties of muscle can be exploited to improve muscular performance during locomotion and other movements. In Chapter 3, we showed that SEEs can function to temporally concentrate energy transfer from the CE to the body and enhance power production during an inertial task like jumping. Applying different neuromuscular strategies that involved antagonistic forces, we measured instantaneous whole muscle power levels that were 2.5 times greater than the maximum power the CE could have produced alone. In Chapter 4, our simulations suggest that SEEs enable the muscle to behave like a spring, recovering over 75% of the kinematic energy from one step and applying it to the next during a steady-state bouncing gait. During locomotion, the neuromuscular system can thus employ control strategies that take advantage of the mechanical properties of muscle to improve energetic efficiency and simplify neural control.

We demonstrated that the CE and SEEs can interact with an external inertia to produce a

dynamically stable bouncing gait, in which energy flows between the inertia and the SEE, and the viscosity of the CE prevents instability. The mathematical three-element model, which was derived from isometric and isokinetic experiments, predicted a stable, resonant system with substantially higher energy conservation than was observed in the closed-loop muscle experiments. The differences between the model predictions and experimental data exemplify the effects of additional properties, apparent only through closed-loop experimental techniques, and not considered in the three-element model. However, the underlying behavior of the model and isolated muscle were qualitatively similar and revealed the autonomous and integrated energy management function of the CE and SEEs.

Our results imply that the optimal neural control strategy requires estimates for muscle mechanical performance and external inertia to coordinate antagonist and agonist muscles. Typical robotic and prosthetic systems often use simplified control methods where one inelastic actuator is used to produce movement in a particular direction. Our results, however, suggest that during inertial tasks like jumping or throwing, antagonist forces play a crucial role in exploiting elastic properties in the agonist muscle and improving performance. To achieve a specific movement, simply activating agonist muscles may not maximize muscular performance. Improving actuator technology to include elastic components and utilizing bioinspired control strategies may improve the performance of engineered systems.

The 'intelligent' mechanical properties of muscle may simplify the control effort required of the central nervous system. In Chapter 4, our results showed that a stable bouncing

gait can be produced by an unvarying motor command, without any sensory feedback, as intrinsic muscle properties automatically produce and dissipate energy to maintain pace. Therefore, the mechanical properties of muscle alone can withstand unexpected mechanical perturbations to the body and maintain dynamic stability. Due to neural time delays, sensory feedback cannot instantaneously respond to mechanical perturbations. During the time delay, however, intrinsic muscular properties can alter the forces produced by the muscle, mitigating the perturbation. Further, the stability provided by the intrinsic properties of muscle implies that the central nervous system may not have to actively control changes in locomotion such as speed. Instead, a single change in muscle activation may be sufficient, as the mechanical properties of muscle may guide the locomotion gait from state to another.

Building actuators with mechanical properties that are similar to that of skeletal muscle may enable robotic systems to match the movement capabilities of animals. We have shown how the dynamic viscous and elastic properties of muscle enable a variety of robust and autonomous functions. Mimicking these properties in artificial actuators may enable robotic systems to better negotiate natural environments. For example, duplicating the viscous and elastic properties of muscle may help robotic systems better respond to high forces that occur during ground contact.

## Model Constraints and Limitations

Our simulation results accurately predicted the kinematics and energetics of isolated muscles during conditions where it only shortened. Previous studies have criticized Hill-type models because they do not explain a variety of nonlinear muscle properties

(Sandercock and Heckman, 1997; Sandercock and Heckman, 2001). During simple shortening movements, however, our model predicted the function of the living muscle with great accuracy. This suggests that nonlinear properties, such as shortening deactivation (Edman et al., 1993; Josephson and Stokes, 1999), may play a small role in some movements and that Hill-type models can accurately predict muscle function during behaviorally relevant tasks.

Mathematical models based on cross-bridge kinetics (Zahalak and Ma, 1990) may be able to better predict the function of living muscle. During movements when the muscle first lengthened before shortening, our results showed that the Hill-type model over predicted the performance of the isolated muscle. During the initial lengthening phase, the model response closely matched the performance of isolated muscle. Throughout the following shortening phase, however, the model force was greater than that produced by the isolated muscle. The source of the hysteretic affect, and other nonlinear muscle properties, cannot be identified using phenomenological Hill-type models. However, cross-bridge muscle models, which mathematically estimate muscle contraction mechanisms, may be able better to identify and predict the effects of muscle nonlinearities on performance. Based on new experimental data, these models can be updated to reflect our improved understanding of muscle contraction mechanisms (Harry et al., 1990). Our closed-loop experimental approach can aid this approach, enabling the study of unknown muscle properties that may arise from dynamic movements and help improve the accuracy of computational muscle models.

The three-element model represents muscle elasticity and viscosity as discrete, series

elements, and has led to the wrong interpretation that series elasticity exists primarily in the tendon or aponeurosis. There are several sites of elasticity throughout the muscle. Intramuscular connective tissue, such as the endomysium, epimysium, and perimysium, has viscoelastic properties. Sarcomereic filaments of actin and myosin also have elastic properties that contribute to the total muscle series elasticity. Thus, muscle viscosity and elasticity are distributed in multiple structural elements, and the three-element model approximates as unitary, independent elements. The semimembranosus was chosen for these experiments because of the lack of external tendon in order to minimize the series compliance. We found over 7% strain associated with elasticity internal to the muscular structure. In contrast, elasticity associated with external tendon and aponeurosis is around 5%/$P_o$, suggesting that non-tendinous elasticity must not be dismissed. SEEs have viscous properties that produce hysteretic effects during stretching and shortening cycles (Lieber et al., 1991). In addition, the stiffness is not constant, but tends to increase with monotonically with increasing length. These nonlinearities likely serve an important functional purpose and may explain the part of the differences we measured between isolated and model muscle.

## Future Directions

Our closed-loop approach has the potential to test hypotheses with real muscles that could previously only be tested with mathematical models. While we demonstrated the benefits of coupling muscle with physical mechanical systems, we did not require this capability to test our scientific hypotheses. There are, however, several forms of locomotion where the interface between the body and the environment is complex and prohibitive to emulate computationally. For example, the function of muscle during

realistic ground contact situations is too complex to mathematically represent and is better simulated with physical models (Altendorfer et al., 2001). As demonstrated in Chapter 2, robotics systems can also include biological elements and better reproduce the interactions that occur during naturally behaving animals. The closed-loop coupling of muscles to robotic systems has an immense potential to improve our understanding of the neuromuscular system and aid in the development of biologically inspired robotic and prosthetic systems.

The effect of sensory mechanisms on muscular mechanics and energetics would be a logical future direction to build upon this thesis. Our closed-loop techniques can be adapted to work with *in vitro* preparations that include intact neural structures. The nonlinear effects of sensory feedback can alter the mechanical properties of muscle. Spinal reflexes, for example, can change the stiffness of lengthening muscles and may play a significant role in maintaining stability during postural balance or locomotion (Nichols and Houk, 1976). During rhythmic movements, neural structures called half centered oscillators have been hypothesized to drive muscles (Williams and DeWeerth, 2007a; Williams and DeWeerth, 2007b). These neural controllers have a variety of feedback mechanisms that enable them to entrain the mechanics of the load and may help improve the stability of the movement. Investigating the role of sensory feedback during locomotion provides a more complete picture of the neuromuscular system's capabilities.

Our closed-loop techniques can be extended so that several antagonistic and agonist muscles can act on a common load. Understanding the synergistic actions of muscles will improve our knowledge on how the neuromuscular system coordinates muscles to

produce a variety of different movements. For example, replacing the idealized antagonistic muscle in Chapter 3 with a real muscle will provide a more accurate estimation of the power generating capabilities of the frog semimembranosus during a co-contraction strategy.

In this research, we investigated the function of the intrinsic properties of a single muscle during a simple, single degree-of-freedom form of locomotion. Ultimately, these methods can be expanded to include neural mechanisms, multiple muscles, and complex mechanics, thereby improving our understanding of the neuromuscular principles that underlie movement.

# REFERENCES


**Ahn, A. N., Monti, R. J. and Biewener, A. A.** (2003). In vivo and in vitro heterogeneity of segment length changes in the semimembranosus muscle of the toad. *Journal of Physiology-London* **549**, 877-888.

**Alexander, R. M. and Bennet-Clark, H. C.** (1977). Storage of Elastic Strain-Energy in Muscle and Other Tissues. *Nature* **265**, 114-117.

**Altendorfer, R., Moore, N., Komsuolu, H., Buehler, M., Brown, H. B., McMordie, D., Saranli, U., Full, R. and Koditschek, D. E.** (2001). RHex: A biologically inspired hexapod runner. *Autonomous Robots* **11**, 207-213.

**Anderson, F. C. and Pandy, M. G.** (1993). Storage and utilization of elastic strain-energy during jumping. *Journal of Biomechanics* **26**, 1413-1427.

**Biewener, A. A. and Gillis, G. B.** (1999). Dynamics of muscle function during locomotion: Accommodating variable conditions. *Journal of Experimental Biology* **202**, 3387-3396.

**Biewener, A. A., Konieczynski, D. D. and Baudinette, R. V.** (1998). In vivo muscle force-length behavior during steady-speed hopping in tammar wallabies. *Journal of Experimental Biology* **201**, 1681-1694.

**Birch, J. M. and Dickinson, M. H.** (2001). Spanwise flow and the attachment of the leading-edge vortex on insect wings. *Nature* **412**, 729-733.

**Blickhan, R.** (1989). The spring mass model for running and hopping. *Journal of Biomechanics* **22**, 1217-1227.

**Blickhan, R., Seyfarth, A., Geyer, H., Grimmer, S., Wagner, H. and Gunther, M.** (2007). Intelligence by mechanics. *Philosophical Transactions of the Royal Society a-Mathematical Physical and Engineering Sciences* **365**, 199-220.

**Caldwell, D. G., Medrano-Cerda, G. A. and Goodwin, M.** (1995). Control of pneumatic muscle actuators. *Control Systems Magazine, IEEE* **15**, 40-48.

**Caldwell, D. G. and Tsagarakis, N.** (2002). Biomimetic actuators in prosthetic and rehabilitation applications. *Technology & Health Care* **10**, 107.

**Cameron, T., Loeb, G. E., Peck, R. A., Schulman, J. H., Strojnik, P. and Troyk, P. R.** (1997). Micromodular implants to provide electrical stimulation of paralyzed muscles and limbs. *Biomedical Engineering, IEEE Transactions on* **44**, 781-790.

**Cavagna, G. A. and Citterio, G.** (1974). Effect of Stretching on Elastic Characteristics and Contractile Component of Frog Striated-Muscle. *Journal of Physiology-London* **239**, 1-14.

**Cavagna, G. A., Heglund, N. C. and Taylor, C. R.** (1977). Mechanical Work in Terrestrial Locomotion - 2 Basic Mechanisms for Minimizing Energy-Expenditure. *American Journal of Physiology* **233**, R243-R261.

**Cavagna, G. A. and Kaneko, M.** (1977). Mechanical Work and Efficiency in Level Walking and Running. *Journal of Physiology-London* **268**, 467-481.

**Cavagna, G. A., Saibene, F. P. and Margaria, R.** (1964). Mechanical work in running. *Journal of Applied Physiology* **19**, 249-&.

**Chizeck, H. J., Crago, P. E. and Kofman, L. S.** (1988). Robust closed-loop control of isometric muscle force using pulsewidth modulation. *Biomedical Engineering, IEEE Transactions on* **35**, 510-517.

**Chizeck, H. J., Lan, N., Palmieri, L. S. and Crago, P. E.** (1991). Feedback control of electrically stimulated muscle using simultaneous pulse width and stimulus period modulation. *Biomedical Engineering, IEEE Transactions on* **38**, 1224-1234.

**Close, R. I.** (1972). Relations between Sarcomere Length and Characteristics of Isometric Twitch Contractions of Frog Sartorius Muscle. *Journal of Physiology-London* **220**, 745-&.

**Crago, P. E., Mortimer, J. T. and Peckham, P. H.** (1980a). Closed-loop control of force during electrical stimulation of muscle. *IEEE Trans Biomed Eng* **27**, 306-12.

**Crago, P. E., Nakai, R. J. and Chizeck, H. J.** (1991). Feedback regulation of hand grasp opening and contact force during stimulation of paralyzed muscle. *Biomedical Engineering, IEEE Transactions on* **38**, 17-28.

**Crago, P. E., Peckham, P. H. and Thrope, G. B.** (1980b). Modulation of Muscle Force by Recruitment During Intramuscular Stimulation. *IEEE Transactions on Biomedical Engineering* **27**, 679-684.

**Daley, M. A. and Biewener, A. A.** (2003). Muscle force-length dynamics during level versus incline locomotion: a comparison of in vivo performance of two guinea fowl ankle extensors. *Journal of Experimental Biology* **206**, 2941-2958.

**Dickinson, M. H., Farley, C. T., Full, R. J., Koehl, M. A. R., Kram, R. and Lehman, S.** (2000). How animals move: An integrative view. *Science* **288**, 100-106.

**Edman, K. A. P., Caputo, C. and Lou, F.** (1993). Depression of Tetanic Force Induced by Loaded Shortening of Frog-Muscle Fibers. *Journal of Physiology-London* **466**, 535-552.

**Farahat, W. and Herr, H.** (2005). An apparatus for characterization and control of isolated muscle. *Neural Systems and Rehabilitation Engineering, IEEE Transactions on [see also IEEE Trans. on Rehabilitation Engineering]* **13**, 473-481.

**Ferris, D. P., Liang, K. L. and Farley, C. T.** (1999). Runners adjust leg stiffness for their first step on a new running surface. *Journal of Biomechanics* **32**, 787-794.

**Ferris, D. P., Louie, M. and Farley, C. T.** (1998). Running in the real world: adjusting leg stiffness for different surfaces. *Proceedings of the Royal Society of London Series B-Biological Sciences* **265**, 989-994.

**Ford, L. E., Huxley, A. F. and Simmons, R. M.** (1977). Tension Responses to Sudden Length Change in Stimulated Frog Muscle-Fibers near Slack Length. *Journal of Physiology-London* **269**, 441-515.

**Full, R. J., Kubow, T., Schmitt, J., Holmes, P. and Koditschek, D.** (2002). Quantifying dynamic stability and maneuverability in legged locomotion. *Integrative and Comparative Biology* **42**, 149-157.

**Gabaldon, A. M., Nelson, F. E. and Roberts, T. J.** (2004). Mechanical function of two ankle extensors in wild turkeys: shifts from energy production to energy absorption during incline versus decline running. *Journal of Experimental Biology* **207**, 2277-2288.

**Gasser, H. S. and Hill, A. V.** (1924). The dynamics of muscular contraction. *Proceedings of the Royal Society of London Series B-Containing Papers of a Biological Character* **96**, 398-436.

**Geyer, H., Seyfarth, A. and Blickhan, R.** (2005). Spring-mass running: simple approximate solution and application to gait stability. *Journal of Theoretical Biology* **232**, 315-328.

**Gillis, G. B.** (2007). The role of hind limb flexor muscles during swimming in the toad, Bufo marinus. *Zoology* **110**, 28-40.

**Gillis, G. B. and Biewener, A. A.** (2000). Hindlimb extensor muscle function during jumping and swimming in the toad (Bufo marinus). *Journal of Experimental Biology* **203**, 3547-+.

**Gordon, A. M., Huxley, A. F. and Julian, F. J.** (1966). The variation in isometric tension with sarcomere length in vertebrate muscle fibres. *Journal of Physiology* **184**, 170-92.

**Gronenberg, W.** (1996). Fast actions in small animals: Springs and click mechanisms. *Journal of Comparative Physiology a-Sensory Neural and Behavioral Physiology* **178**, 727-734.

**Harry, J. D., Ward, A. W., Heglund, N. C., Morgan, D. L. and McMahon, T.**

**A.** (1990). Cross-Bridge Cycling Theories Cannot Explain High-Speed Lengthening Behavior In Frog-Muscle. *Biophysical Journal* **57**, 201-208.

**Herr, H. and Dennis, R. G.** (2004). A swimming robot actuated by living muscle tissue. *J Neuroengineering Rehabil* **1**, 6.

**Herr, H., Pratt, G., Dennis, R., Rosental, N. and Marsh, R.** (2001). From Swimming to Walking: Examples of How Biology is Helping us Design Better Machines. In *Motion Systems*. University of Jena, Jena, Germany.

**Higuchi, H., Yanagida, T. and Goldman, Y. E.** (1995). Compliance of thin filaments in skinned fibers of rabbit skeletal muscle. *Biophys. J.* **69**, 1000-1010.

**Hill, A. V.** (1938). The heat of shortening and the dynamic constants of muscle. *Proceedings of the Royal Society of London Series B-Biological Sciences* **126**, 136-195.

**Hirano, M. and Rome, L. C.** (1984). Jumping Performance of Frogs (Rana-Pipiens) as a Function of Muscle Temperature. *Journal of Experimental Biology* **108**, 429-439.

**Houk, J. C., Rymer, W. Z. and Crago, P. E.** (1981). Dependence of Dynamic-Response of Spindle Receptors on Muscle Length and Velocity. *Journal of Neurophysiology* **46**, 143-166.

**Huxley, A. F.** (1957). Muscle Structure and Theories of Contraction. *Progress in Biophysics & Molecular Biology* **7**, 255-&.

**Huxley, H. E., Stewart, A., Sosa, H. and Irving, T.** (1994). X-ray diffraction measurements of the extensibility of actin and myosin filaments in contracting muscle. *Biophys. J.* **67**, 2411-2421.

**Johansson, L. C. and Lauder, G. V.** (2004). Hydrodynamics of surface swimming in leopard frogs (Rana pipiens). *Journal of Experimental Biology* **207**, 3945-3958.

**Johnston, T. E., Betz, R. R., Smith, B. T. and Mulcahey, M. J.** (2003). Implanted functional electrical stimulation: an alternative for standing and walking in pediatric spinal cord injury. *Spinal Cord* **41**, 144-52.

**Josephson, R. K.** (1985). Mechanical Power Output from Striated-Muscle During Cyclic Contraction. *Journal of Experimental Biology* **114**, 493-512.

**Josephson, R. K.** (1993). Contraction Dynamics and Power Output of Skeletal-Muscle. *Annual Review of Physiology* **55**, 527-546.

**Josephson, R. K.** (1999). Dissecting muscle power output. *Journal of Experimental Biology* **202**, 3369-3375.

**Josephson, R. K. and Stokes, D. R.** (1999). Work-dependent deactivation of a crustacean muscle. *Journal of Experimental Biology* **202**, 2551-2565.

**Julian, F. J., Rome, L. C., Stephenson, D. G. and Striz, S.** (1986). The Maximum Speed of Shortening in Living and Skinned Frog-Muscle Fibers. *Journal of Physiology-London* **370**, 181-&.

**Kamel, L. T., Peters, S. E. and Bashor, D. P.** (1996). Hopping and swimming in the leopard frog, Rana pipiens .2. A comparison of muscle activities. *Journal of Morphology* **230**, 17-31.

**Kargo, W. J. and Rome, L. C.** (2002). Functional morphology of proximal hindlimb muscles in the frog Rana pipiens. *Journal of Experimental Biology* **205**, 1987-2004.

**Katz, B.** (1939). The relation between force and speed in muscular contraction. *Journal of Physiology-London* **96**, 45-64.

**Kawakami, Y. and Lieber, R. L.** (2000). Interaction between series compliance and sarcomere kinetics determines internal sarcomere shortening during fixed-end contraction. *Journal of Biomechanics* **33**, 1249-1255.

**Lan, N., Crago, P. E. and Chizeck, H. J.** (1991). Feedback control methods for task regulation by electrical stimulation of muscles. *Biomedical Engineering, IEEE Transactions on* **38**, 1213-1223.

**Lau, B., Guevremont, L. and Mushahwar, V. K.** (2007). Strategies for generating prolonged functional standing using intramuscular stimulation or entraspinal microstimulation. *Ieee Transactions on Neural Systems and Rehabilitation Engineering* **15**, 273-285.

**Lemay, M. A., Crago, P. E., Katorgi, M. and Chapman, G. J.** (1993). Automated tuning of a closed-loop hand grasp neuroprosthesis. *Biomedical Engineering, IEEE Transactions on* **40**, 675-685.

**Lieber, R. L., Leonard, M. E., Brown, C. G. and Trestik, C. L.** (1991). Frog Semitendinosis Tendon Load-Strain and Stress-Strain Properties During Passive Loading. *American Journal of Physiology* **261**, C86-C92.

**Lin, D. C. and Rymer, W. Z.** (1998). Damping in reflexively active and areflexive lengthening muscle evaluated with inertial loads. *Journal of Neurophysiology* **80**, 3369-3372.

**Lin, D. C. and Rymer, W. Z.** (2000). Damping actions of the neuromuscular system with inertial loads: soleus muscle of the decerebrate cat. *J Neurophysiol* **83**, 652-8.

**Lin, D. C. and Rymer, W. Z.** (2001). Damping Actions of the Neuromuscular

System With Inertial Loads: Human Flexor Pollicis Longus Muscle. *J Neurophysiol* **85**, 1059-1066.

**Loeb, G. E., Brown, I. E. and Cheng, E. J.** (1999). A hierarchical foundation for models of sensorimotor control. *Experimental Brain Research* **126**, 1-18.

**Loeb, G. E. and Davoodi, R.** (2005). The functional reanimation of paralyzed limbs. *Engineering in Medicine and Biology Magazine, IEEE* **24**, 45-51.

**Lutz, G. J. and Rome, L. C.** (1994). Built for Jumping - the Design of the Frog Muscular System. *Science* **263**, 370-372.

**Lutz, G. J. and Rome, L. C.** (1996a). Muscle function during jumping in frogs .1. Sarcomere length change, EMG pattern, and jumping performance. *American Journal of Physiology-Cell Physiology* **40**, C563-C570.

**Lutz, G. J. and Rome, L. C.** (1996b). Muscle function during jumping in frogs .2. Mechanical properties of muscle: Implications for system design. *American Journal of Physiology-Cell Physiology* **40**, C571-C578.

**Lyons, G. M., Sinkjaer, T., Burridge, J. H. and Wilcox, D. J.** (2002). A review of portable FES-based neural orthoses for the correction of drop foot. *IEEE Trans Neural Syst Rehabil Eng* **10**, 260-79.

**Marsh, R. L.** (1999). How muscles deal with real-world loads: The influence of length trajectory on muscle performance. *Journal of Experimental Biology* **202**, 3377-3385.

**McDonnall, D., Clark, G. A. and Normann, K. A.** (2004). Interleaved, multisite electrical stimulation of cat sciatic nerve produces fatigue-resistant, ripple-free motor responses. *Ieee Transactions on Neural Systems and Rehabilitation Engineering* **12**, 208-215.

**McMahon, T. A. and Cheng, G. C.** (1990). The mechanics of running: How does stiffness couple with speed? *Journal of Biomechanics* **23**, 65-78.

**Meijer, K., Bar-Cohen, Y. and Full, R. J.** (2003). Biological Inspiration for Musclelike Actuators of Robots. In *Biologically inspired intelligent robots*, eds. Y. Bar-Cohen and C. Breazeal), pp. 25-45. Bellingham: SPIE-The International Society for Optical Engineering.

**Migliore, S. A., Brown, E. A. and DeWeerth, S. P.** (2007). Novel nonlinear elastic actuators for passively controlling robotic joint compliance. *Journal of Mechanical Design* **129**, 406-412.

**Nauwelaerts, S. and Aerts, P.** (2003). Propulsive impulse as a covarying performance measure in the comparison of the kinematics of swimming and jumping in frogs. *Journal of Experimental Biology* **206**, 4341-4351.

**Nauwelaerts, S. and Aerts, P.** (2006). Take-off and landing forces in jumping frogs. *Journal of Experimental Biology* **209**, 66-77.

**Nauwelaerts, S., Stamhuis, E. and Aerts, P.** (2005). Swimming and jumping in a semi-aquatic frog. *Animal Biology* **55**, 3-15.

**Nichols, T. R. and Houk, J. C.** (1976). Improvement in linearity and regulation of stiffness that results from actions of stretch reflex. *J Neurophysiol* **39**, 119-142.

**Olson, J. M. and Marsh, R. L.** (1998). Activation patterns and length changes in hindlimb muscles of the bullfrog Rana catesbeiana during jumping. *Journal of Experimental Biology* **201**, 2763-2777.

**Peckham, P. H. and Knutson, J. S.** (2005). Functional Electrical Stimulation For Neuromuscular Applications. *Annual Review of Biomedical Engineering* **7**, 327-360.

**Peplowski, M. M. and Marsh, R. L.** (1997). Work and power output in the hindlimb muscles of Cuban tree frogs Osteopilus septentrionalis during jumping. *Journal of Experimental Biology* **200**, 2861-2870.

**Peters, S. E., Kamel, L. T. and Bashor, D. P.** (1996). Hopping and swimming in the leopard frog, Rana pipiens .1. Step cycles and kinematics. *Journal of Morphology* **230**, 1-16.

**Popovic, M. B.** (2003). Control of neural prostheses for grasping and reaching. *Medical Engineering and Physics* **25**, 41-50.

**Popovic, M. R., Curt, A., Keller, T. and Dietz, V.** (2001). Functional electrical stimulation for grasping and walking: indications and limitations. *Spinal Cord* **39**, 403-12.

**Pratt, G. A.** (2000). Legged robots at MIT: what's new since Raibert? *Robotics & Automation Magazine, IEEE* **7**, 15-19.

**Pratt, G. A.** (2002). Low impedance walking robots. *Integrative and Comparative Biology* **42**, 174-181.

**Roberts, T. J.** (2002). The integrated function of muscles and tendons during locomotion. *Comparative Biochemistry and Physiology a-Molecular and Integrative Physiology* **133**, 1087-1099.

**Roberts, T. J. and Marsh, R. L.** (2003). Probing the limits to muscle-powered accelerations: lessons from jumping bullfrogs. *Journal of Experimental Biology* **206**, 2567-2580.

**Roberts, T. J., Marsh, R. L., Weyand, P. G. and Taylor, C. R.** (1997). Muscular force in running turkeys: The economy of minimizing work. *Science* **275**, 1113-1115.

**Roberts, T. J. and Scales, J. A.** (2002). Mechanical power output during running accelerations in wild turkeys. *Journal of Experimental Biology* **205**, 1485-1494.

**Rome, L. C., Funke, R. P., Alexander, R. M., Lutz, G., Aldridge, H., Scott, F. and Freadman, M.** (1988). Why Animals Have Different Muscle-Fiber Types. *Nature* **335**, 824-827.

**Rome, L. C., Sosnicki, A. and Choi, I. H.** (1992). The Influence of Temperature on Muscle Function in the Fast Swimming Scup .2. the Mechanics of Red Muscle. *Journal of Experimental Biology* **163**, 281-295.

**Rome, L. C. and Sosnicki, A. A.** (1990). The Influence of Temperature on Mechanics of Red Muscle in Carp. *Journal of Physiology-London* **427**, 151-169.

**Rome, L. C. and Swank, D.** (1992). The Influence of Temperature on Power Output of Scup Red Muscle During Cyclical Length Changes. *Journal of Experimental Biology* **171**, 261-281.

**Sandercock, T. G. and Heckman, C. J.** (1997). Force from cat soleus muscle during imposed locomotor-like movements: Experimental data versus hill-type model predictions. *Journal of Neurophysiology* **77**, 1538-1552.

**Sandercock, T. G. and Heckman, C. J.** (2001). Whole muscle length-tension properties vary with recruitment and rate modulation in areflexive cat soleus. *Journal of Neurophysiology* **85**, 1033-1038.

**Scrivens, J. E., DeWeerth, S. P. and Ting, L. H.** (2008). A robotic device for understanding neuromechanical interactions during standing balance control. *Bioinspiration & Biomimetics* **3**.

**Seyfarth, A., Geyer, H., Gunther, M. and Blickhan, R.** (2002). A movement criterion for running. *Journal of Biomechanics* **35**, 649-655.

**Seyfarth, A., Geyer, H. and Heff, H.** (2003). Swing-leg retraction: a simple control model for stable running. *Journal of Experimental Biology* **206**, 2547-2555.

**Shadmehr, R. and Arbib, M. A.** (1992). A mathematical analysis of the force-stiffness characteristics of muscles in control of a single joint system. *Biol Cybern* **66**, 463-77.

**Stevens, E. D.** (1996). The pattern of stimulation influences the amount of oscillatory work done by frog muscle. *Journal of Physiology-London* **494**, 279-285.

**Trinh, M. and Syme, D. A.** (2007). Effects of stretch on work and efficiency of frog ( Rana pipiens) muscle. *Journal of Experimental Biology* **210**, 2843-2850.

**Wagner, H. and Blickhan, R.** (1999). Stabilizing function of skeletal muscles: an analytical investigation. *Journal of Theoretical Biology* **199**, 163-179.

**Weber, D. J., Stein, R. B., Chan, K. M., Loeb, G., Richmond, F., Rolf, R., James, K. and Su Ling, C.** (2005). BIONic WalkAide for correcting foot drop. *Neural Systems and Rehabilitation Engineering, IEEE Transactions on [see also IEEE Trans. on Rehabilitation Engineering]* **13**, 242-246.

**Wieler, M., Stein, R. B., Ladouceur, M., Whittaker, M., Smith, A. W., Naaman, S., Barbeau, H., Bugaresti, J. and Aimone, E.** (1999). Multicenter evaluation of electrical stimulation systems for walking. *Arch Phys Med Rehabil* **80**, 495-500.

**Williams, C. A. and DeWeerth, S. P.** (2007a). A comparison of resonance tuning with positive versus negative sensory feedback. *Biological Cybernetics* **96**, 603-614.

**Williams, C. A. and DeWeerth, S. P.** (2007b). Resonance tuning of a neuromechanical system with two negative sensory feedback configurations, pp. 1954-1959: Elsevier Science Bv.

**Zahalak, G. I. and Ma, S. P.** (1990). Muscle Activation and Contraction - Constitutive Relastions Based Directly On Cross-Bridge Kinetics. *Journal of Biomechanical Engineering-Transactions of the Asme* **112**, 52-62.

**Zajac, F. E.** (1989). Muscle and Tendon - Properties, Models, Scaling, and Application to Biomechanics and Motor Control. *Critical Reviews in Biomedical Engineering* **17**, 359-411.

# VITA

## KARTIK SUNDAR

Kartik was born in Bombay, India in 1980 but spent his childhood in the Middle East. He moved to Toronto, Canada in 1993 where he attended Unionville High School. In May 2003, Kartik received a B.Sc in Applied Mathematics from Queen's University, Kingston, Ontario. In August 2003, Kartik enrolled in the Ph.D. Bioengineering program at the Georgia Institute of Technology, Atlanta, GA. While completing his Ph.D., Kartik also earned a M.S. in Electrical Engineering. Kartik completed his dissertation in January 2009. He currently works as a management consultant in Atlanta.